



## Research paper

# Spinel structured $\text{Co}_a\text{Mn}_b\text{O}_x$ mixed oxide catalyst for the selective catalytic reduction of $\text{NO}_x$ with $\text{NH}_3$

Dongmei Meng, Qian Xu, Yunlei Jiao, Yun Guo, Yanglong Guo, Li Wang, Guanzhong Lu\*, Wangcheng Zhan\*



Key Laboratory for Advanced Materials and Research Institute of Industrial Catalysis, School of Chemistry and Molecular Engineering, East China University of Science and Technology, 130 Meilong Road, Shanghai, 200237, PR China

## ARTICLE INFO

## Keywords:

Mixed oxide  
Selective catalytic reduction  
Spinel structure  
Thermal stability  
Synergistic effect

## ABSTRACT

A highly efficient catalyst of a  $\text{Co}_a\text{Mn}_b\text{O}_x$  mixed oxide prepared by the co-precipitation method was developed for the selective catalytic reduction (SCR) of  $\text{NO}_x$  with ammonia. With an increase in the Mn content, the catalytic activity of the  $\text{Co}_a\text{Mn}_b\text{O}_x$  mixed oxide exhibited a volcano-type tendency, and when  $\text{Co}/\text{Mn}$  molar ratio reached 7:3 ( $\text{Co}_7\text{Mn}_3\text{O}_x$ ), the operation temperature for achieving  $> 80\%$   $\text{NO}_x$  conversion was 170 °C (116–285 °C window). The formation of spinel structured  $\text{MnCo}_2\text{O}_4$  is highly important, and the presence of the spinel structure in  $\text{Co}_7\text{Mn}_3\text{O}_x$  contributes to the increase in active sites and thermal stability and promotes  $\text{SO}_2$  and/or  $\text{H}_2\text{O}$  resistance. In comparison with  $\text{MnO}_x$  or  $\text{CoO}_x$  alone, the  $\text{Co}_a\text{Mn}_b\text{O}_x$  catalysts possess improved redox properties and more surface acid sites due to synergistic effects between the Co and Mn species. Among the  $\text{Co}_a\text{Mn}_b\text{O}_x$  catalysts with different Co/Mn molar ratios, a higher  $\text{NH}_3$  and  $\text{NO} + \text{O}_2$  adsorption ability was found for the  $\text{Co}_7\text{Mn}_3\text{O}_x$  catalyst, originating from its  $\text{MnCo}_2\text{O}_{4.5}$  phase and higher surface area, which leads to the higher activity of the  $\text{Co}_7\text{Mn}_3\text{O}_x$  catalyst. In situ DRIFTS indicated that bridging nitrate and bidentate nitrate are the intermediate species in the  $\text{NH}_3$ -SCR reaction, and the high NO adsorption ability and improved redox properties of the  $\text{Co}_7\text{Mn}_3\text{O}_x$  catalyst are beneficial for the formation of nitrate species on the catalyst surface. Furthermore,  $\text{NH}_3$  species adsorbed at Lewis acid sites taken part in SCR reaction, while the reactivity of  $\text{NH}_3$  species adsorbed at Brønsted acid was not definitized.

## 1. Introduction

The emission of nitrogen oxides generated by power stations and mobile resources is regarded as a dominant contributor to atmospheric pollution [1,2], which can cause haze and acid rain, boost the photochemical chain reaction to form photochemical smog, aggravate the greenhouse effect, and injure the human respiratory system. Therefore, the control of  $\text{NO}_x$  emission has already attracted the world's attention. Consequently, many countries have established various standards to control  $\text{NO}_x$  emissions from power stations and mobile resources.

The selective catalytic reduction of  $\text{NO}_x$  with  $\text{NH}_3$  ( $\text{NH}_3$ -SCR) has been regarded as an efficient approach to eliminate  $\text{NO}_x$  in the presence of excess oxygen [3]. Many types of catalysts have been studied for the  $\text{NH}_3$ -SCR reaction, among which commercially available vanadium-based mixed oxides and transition metal-exchanged zeolite catalysts are more widely used. Although vanadium-based SCR catalysts show high performance at 300–400 °C [4,5], they have some inherent disadvantages in practical applications, such as the narrow operation

temperature window, the high conversion of  $\text{SO}_2$  to  $\text{SO}_3$  at high temperatures and the toxicity of vanadium pentoxide to the environment and human health. Transition metal-exchanged zeolites [6–8] usually exhibit a wide operation temperature window at 250–600 °C and satisfactory de- $\text{NO}_x$  efficiency. However, their hydrothermal stability is a great challenge for the large-scale application of zeolite-based catalysts. What is worse, when treating stack gases from stationary sources (accounting for approximately 46% of  $\text{NO}_x$  emission [9]), the gas temperature is usually low after passing through the sweetener and dust separation plant to eliminate  $\text{SO}_x$  and solid particles in the stack gases. Therefore, the study of SCR catalysts with excellent performance at low temperature (< 250 °C) has attracted much attention [10,11].

Some transition metal oxides have been proven to be effective for low-temperature  $\text{NH}_3$ -SCR, especially manganese-based catalysts [12–14]. However, the catalytic activity of manganese oxides decreases dramatically at higher temperatures [15], where its structure, shape, valence state and surface area are changed, leading to a decrease in its catalytic activity for the  $\text{NH}_3$ -SCR reaction [16,17]. As is well known,

\* Corresponding authors.

E-mail addresses: [gzhlu@ecust.edu.cn](mailto:gzhlu@ecust.edu.cn) (G. Lu), [zhanwc@ecust.edu.cn](mailto:zhanwc@ecust.edu.cn) (W. Zhan).

perovskite, spinel and pyrochlore are typical structures of metal oxides with high stability. Since the low surface area of perovskite and pyrochlore is the most fatal disadvantage in the NH<sub>3</sub>-SCR reaction, we used spinel structured oxide as the catalyst for NH<sub>3</sub>-SCR. The introduction of a secondary element into transition metal oxides can modulate the ionic properties of the metal and increase the amount of surface defects on the oxides, thus promoting the efficiency of the transition metal oxide for the catalytic abatement of NO<sub>x</sub> in the NH<sub>3</sub>-SCR reaction with acid and redox cycles. Previous research has revealed that Co-Mn mixed oxides exhibit good redox ability and high catalytic activity in oxidative reactions, such as CO oxidation, HC and VOC combustions [18–20], which is a very important factor for NH<sub>3</sub>-SCR. To promote the catalytic performance and simultaneously weaken the high-temperature sensitivity of manganese-based catalysts, spinel structured Co-Mn mixed oxides have great potential for development as a result of synergistic effects between manganese and cobalt, due to the high activity of Co<sub>3</sub>O<sub>4</sub> for the NH<sub>3</sub>-SCR reaction [17] and the similar ionic radii of Co and Mn (Co<sup>3+</sup> = 0.63 Å, Co<sup>2+</sup> = 0.72 Å, Mn<sup>4+</sup> = 0.60 Å and Mn<sup>3+</sup> = 0.66 Å).

Herein, spinel structured Co<sub>a</sub>Mn<sub>b</sub>O<sub>x</sub> catalysts were synthesized by the co-precipitation method, and the effects of the Co/Mn molar ratio on the structure and physicochemical properties and the catalytic performances of Co<sub>a</sub>Mn<sub>b</sub>O<sub>x</sub> mixed oxides for low-temperature NH<sub>3</sub>-SCR were systematically investigated by various characterization methods. Meanwhile, NH<sub>3</sub>-TPD, NO-TPD and *in situ* DRIFTS (diffuse reflectance infrared Fourier transform spectroscopy) were used to reveal the adsorption of reactants and the surface reactions of the adsorbed reactants. Subsequently, the mechanism of NH<sub>3</sub>-SCR over the Co<sub>7</sub>Mn<sub>3</sub>O<sub>x</sub> catalyst and the synergistic catalytic effect between the Mn and Co cations were explicitly discussed.

## 2. Experimental

### 2.1. Catalyst preparation

The Co<sub>a</sub>Mn<sub>b</sub>O<sub>x</sub> catalysts were synthesized by the co-precipitation method. MnSO<sub>4</sub> and Co(NO<sub>3</sub>)<sub>2</sub>·6H<sub>2</sub>O were used as salt precursors, and Na<sub>2</sub>CO<sub>3</sub> solution was utilized as the precipitant. Typically, the desired amount of MnSO<sub>4</sub> and Co(NO<sub>3</sub>)<sub>2</sub>·6H<sub>2</sub>O were dissolved in 100 mL of deionized water at room temperature. Then, this mixed solution and a 0.2 M Na<sub>2</sub>CO<sub>3</sub> solution were added dropwise to a beaker at the same time under stirring, and the pH value of the system was maintained at 9. After being stirred for 24 h, the solid product was collected by filtration, dried at 120 °C for 12 h, and finally calcined in air at 550 °C for 4 h at a heating rate of 2 °C/min. All prepared catalysts were designated Co<sub>a</sub>Mn<sub>b</sub>O<sub>x</sub>, where a/b is the ideal relative molar ratio of Co/Mn. For example, 2.26 g of MnSO<sub>4</sub> and 10.18 g of Co(NO<sub>3</sub>)<sub>2</sub>·6H<sub>2</sub>O was employed when producing Co<sub>7</sub>Mn<sub>3</sub>O<sub>x</sub>. In addition, CoO<sub>x</sub> and MnO<sub>x</sub> samples were prepared using the same method without the addition of the second metal.

A Co-Mn mixed oxide catalyst (Co/Mn mole ratio was the same as Co<sub>7</sub>Mn<sub>3</sub>O<sub>x</sub>) was also prepared by a two-step precipitation method as follows. 10.18 g of Co(NO<sub>3</sub>)<sub>2</sub>·6H<sub>2</sub>O and 2.26 g of MnSO<sub>4</sub> were dissolved in 50 mL of deionized water separately. Co(NO<sub>3</sub>)<sub>2</sub> solution and 0.2 M NaCO<sub>3</sub> solution were slowly added dropwise to a beaker with 100 mL of water, and the pH value was kept at 9. After stirring for 2 h, the MnSO<sub>4</sub> solution was added dropwise to the above precipitated solution along with a 0.2 M NaCO<sub>3</sub> solution. The following preparation process was the same as that for preparing the Co<sub>a</sub>Mn<sub>b</sub>O<sub>x</sub> catalysts, and the obtained catalyst was denoted CoO<sub>x</sub>@MnO<sub>x</sub>. Meanwhile, a Co-Mn mixed oxide was prepared in reverse order, i.e., MnSO<sub>4</sub> solution and 0.2 M NaCO<sub>3</sub> solution were precipitated first and then Co(NO<sub>3</sub>)<sub>2</sub> solution was added into the above mixture along with a 0.2 M NaCO<sub>3</sub> solution. The obtained catalyst was denoted MnO<sub>x</sub>@CoO<sub>x</sub>.

### 2.2. Catalyst characterization

The XRD measurement was conducted on a Brook/D8 diffractometer employing Cu K $\alpha$  radiation. The diffraction patterns were obtained in the 2θ range of 10–80° with a step size of 0.06°. The crystalline phase was confirmed through comparison with the reference data from ICDD files. Transmission electron microscopy (TEM) of the samples was carried out on a JEOL 2100F electron microscope operated at 200 kV. The N<sub>2</sub> adsorption-desorption isotherms were measured on a Micromeritics ASAP 2020 M surface area and pore size analyzer. Before the measurements, all samples were degassed at 180 °C until a stable vacuum of ca. 5 mTorr was reached. The specific surface area was calculated from desorption data by the Brunauer-Emmett-Teller (BET) method. The XPS spectra were obtained on a Thermo ESCALAB 250 spectrometer with Al K $\alpha$  radiation. The C 1 s line at 284.6 eV from contaminant carbon was defined as the reference.

The temperature-programmed desorption of NH<sub>3</sub> (NH<sub>3</sub>-TPD) was conducted on a PX200 apparatus (Tianjin Pengxiang Technology Limited Corporation) with a thermal conductivity detector (TCD). For this, 100 mg of catalyst was added to the quartz reactor and then pretreated at 450 °C in a flow of N<sub>2</sub> (50 mL/min) for 1 h. When being cooled to room temperature, the sample was exposed to a flow of 10% NH<sub>3</sub>/N<sub>2</sub> (50 mL/min) for 1 h. After the sample was flushed with N<sub>2</sub> (50 mL/min) for 1 h, NH<sub>3</sub>-TPD was carried out at a heating rate of 10 °C/min in N<sub>2</sub> (50 mL/min) from room temperature to 450 °C.

The O<sub>2</sub>-TPD-MS experiment was implemented on an automatic chemical adsorption instrument (Micromeritics Autochem ii 2920) equipped with a U-shaped quartz reactor and a mass spectrometer (HIDEN HPR 20). For this, 50 mg of sample was pretreated at 250 °C in He for 30 min and in 3% O<sub>2</sub>/He for another 30 min consecutively and then cooled down to 30 °C in 3% O<sub>2</sub>/He. After the catalyst was kept in He for 1 h, O<sub>2</sub>-TPD was run from 30 °C to 600 °C at a rate of 10 °C/min.

The temperature-programmed desorption of NO<sub>x</sub> (NO<sub>x</sub>-TPD) was performed on custom-made equipment with an NO<sub>x</sub> analyzer (Thermo Fisher 42i-HL-NO-NO<sub>x</sub> analyzer) as the detector. The sample was pretreated in 5 vol.% O<sub>2</sub>/Ar (300 mL/min) at 450 °C for 1 h and then cooled to room temperature. Then, the sample was exposed to a flow of 500 ppm NO/5 vol.% O<sub>2</sub>/Ar (300 mL/min) for 1 h (when the NO<sub>x</sub> on the samples reached a saturated state), followed by Ar (300 mL/min) purge for 1 h. Finally, TPD was run by heating the sample in Ar (300 mL/min) from room temperature to 450 °C at 10 °C/min.

Temperature-programmed reduction of H<sub>2</sub> (H<sub>2</sub>-TPR) experiments were also conducted on a PX200 apparatus with a TCD. For this, 50 mg of sample was directly heated from room temperature to 600 °C at a rate of 10 °C/min in a flow of 5 vol.% H<sub>2</sub>/N<sub>2</sub> (45 mL/min). The hydrogen consumption was quantitatively evaluated by the TCD signal.

*In situ* DRIFT measurements were performed on a Nicolet 6700 FT-IR spectrometer with an MCT detector. In the DRIFT cell, containing ZnSe windows and a connected gas flow system, the sample was pretreated at 450 °C in 5 vol.% O<sub>2</sub>/Ar for 1 h and then cooled to 20 °C in Ar. The background spectra were collected at certain temperatures during the cooling process, and these background spectra was subtracted from sample spectra accordingly.

### 2.3. Catalytic activity testing

The catalytic performances of the catalysts for NH<sub>3</sub>-SCR were detected in a continuous-flow fixed-bed quartz reactor at atmospheric pressure. For this, 300 mg of the catalyst (40–60 mesh) was used, and the reactant gas included 500 ppm NO, 500 ppm NH<sub>3</sub>, 5 vol.% H<sub>2</sub>O (when used), 5 vol.% O<sub>2</sub> and Ar as the balanced gas. The gas hourly space velocity (GHSV) was 80,000 h<sup>-1</sup>. The concentrations of NO and NO<sub>2</sub> in the gas mixture before and after the reaction were analyzed using the NO<sub>x</sub> analyzer (Thermo Fisher 42i-HL-NO-NO<sub>x</sub> analyzer). Because the oxidation of ammonia in the chamber of the NO/NO<sub>x</sub> analyzer may cause an unexpected generation of NO<sub>x</sub>, an ammonia trap

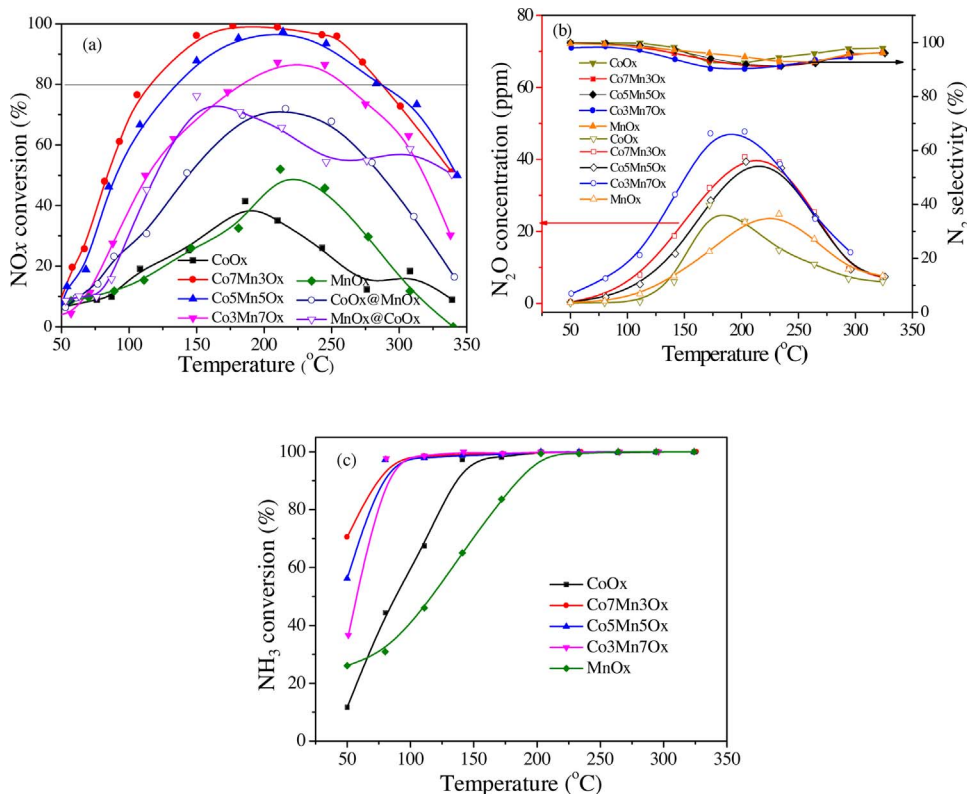


**Fig. 1.** Catalytic performances of the MnO<sub>x</sub>, CoO<sub>x</sub>, Co-Mn-O<sub>x</sub>, Mn-Co-O<sub>x</sub> and Co<sub>a</sub>Mn<sub>b</sub>O<sub>x</sub> catalysts for the NH<sub>3</sub>-SCR reaction, including NO<sub>x</sub> conversion (a), N<sub>2</sub> selectivity along with N<sub>2</sub>O concentration (b), as well as NH<sub>3</sub> conversion (c), as a function of temperature. (Reaction conditions: 0.3 g of sample, 500 ppm NO + 500 ppm NH<sub>3</sub> + 5 vol.% H<sub>2</sub>O + 5 vol.% O<sub>2</sub>/Ar balanced, total flow rate 300 mL/min and GHSV = 80000 h<sup>-1</sup>).

containing phosphoric acid solution was installed prior to the analyzer. N<sub>2</sub>O and NH<sub>3</sub> were monitored by a Nicolet 6700 FT-IR spectrometer with an MCT detector. NO<sub>x</sub> conversion ( $x(\text{NO}_x)$ ) and N<sub>2</sub> selectivity ( $S(\text{N}_2)$ ) were calculated as follows:

$$x(\text{NO}_x) = \frac{C(\text{NO}_x)_{\text{in}} - C(\text{NO}_x)_{\text{out}}}{C(\text{NO}_x)_{\text{in}}} \times 100\%$$

$$S(\text{N}_2) = \frac{C(\text{NO}_x)_{\text{in}} + C(\text{NH}_3)_{\text{in}} - C(\text{NO}_x)_{\text{out}} - C(\text{NH}_3)_{\text{out}} - 2C(\text{N}_2\text{O})_{\text{out}}}{C(\text{NO}_x)_{\text{in}} + C(\text{NH}_3)_{\text{in}} - C(\text{NO}_x)_{\text{out}} - C(\text{NH}_3)_{\text{out}}} \times 100\%$$

$C(\text{NO}_x)_{\text{in}}$  and  $C(\text{NO}_x)_{\text{out}}$  are the concentrations of NO<sub>x</sub> in the inlet and outlet, respectively.  $C(\text{NH}_3)_{\text{in}}$  and  $C(\text{NH}_3)_{\text{out}}$  are the concentrations of NH<sub>3</sub> in the inlet and outlet, respectively.  $C(\text{N}_2\text{O})$  is the concentration of N<sub>2</sub>O generated during the reaction process.

### 3. Results and discussion

#### 3.1. Effect of the Co/Mn molar ratio on the catalytic activity

Fig. 1a shows NO<sub>x</sub> conversion as a function of temperature in the NH<sub>3</sub>-SCR reaction over the MnO<sub>x</sub>, CoO<sub>x</sub> and Co<sub>a</sub>Mn<sub>b</sub>O<sub>x</sub> catalysts. A bimodal curve of NO<sub>x</sub> conversion with NO<sub>x</sub> conversions of 41% (at 185 °C) and 18% (at 305 °C) can be observed over the CoO<sub>x</sub> catalyst. Compared with CoO<sub>x</sub>, MnO<sub>x</sub> showed higher activity, over which ~54% NO<sub>x</sub> conversion was achieved at 223 °C. However, the combination of Mn and Co to form a mixed oxide can dramatically enhance the NH<sub>3</sub>-SCR catalytic performance, which is dependent on the Co/Mn molar ratio. When the molar ratio of Co/Mn is 7/3, the Co<sub>7</sub>Mn<sub>3</sub>O<sub>x</sub> catalyst showed the best NH<sub>3</sub>-SCR activity with an operation temperature window (80% NO<sub>x</sub> conversion) of 116–285 °C, which is much better than the catalysts with Co/Mn molar ratios of 5/5 and 3/7. Additionally, the activity of the Co<sub>7</sub>Mn<sub>3</sub>O<sub>x</sub> catalyst is also much higher than that of the CoO<sub>x</sub>@MnO<sub>x</sub> and MnO<sub>x</sub>@CoO<sub>x</sub> catalysts with the same Co/Mn molar ratio, which were prepared by the two-step precipitation method, indicating that the existence of synergistic effects between Co

and Mn oxide in the Co<sub>7</sub>Mn<sub>3</sub>O<sub>x</sub> catalyst can obviously increase the catalytic activity of both MnO<sub>x</sub> and CoO<sub>x</sub>. N<sub>2</sub> selectivity along with the N<sub>2</sub>O concentration, and NH<sub>3</sub> conversion as a function of temperature were also provided in Fig. 1b and c. All catalysts exhibited a high N<sub>2</sub> selectivity in the temperature range of 50–325 °C. However, N<sub>2</sub>O concentration showed a volcano-type tendency over all catalysts and it reached the maximum at about 200 °C. Furthermore, the highest value of N<sub>2</sub>O concentration decreased in the order of Co<sub>3</sub>Mn<sub>7</sub>O<sub>x</sub> > Co<sub>7</sub>Mn<sub>3</sub>O<sub>x</sub> > Co<sub>5</sub>Mn<sub>5</sub>O<sub>x</sub> > CoO<sub>x</sub> ≈ MnO<sub>x</sub>. As for NH<sub>3</sub> conversion, it can reach 100% at 75 °C over the Co<sub>a</sub>Mn<sub>b</sub>O<sub>x</sub> catalysts, indicating a high utilization of NH<sub>3</sub> for SCR reaction at low temperature. On the contrary, the temperature for NH<sub>3</sub> conversion of 100% increased to 200 °C over the CoO<sub>x</sub> and MnO<sub>x</sub> catalysts, due to their low catalytic activity for SCR reaction at low temperature, as shown in Fig. 1a.

The SCR activity is further studied to obtain information on the reaction kinetics, in which the NO<sub>x</sub> conversion is less than 20%. The energy barrier and Arrhenius plot are presented in Fig. 2. It can be found that the rate constant increased in the order of MnO<sub>x</sub> < Co<sub>3</sub>Mn<sub>7</sub>O<sub>x</sub> < Co<sub>5</sub>Mn<sub>5</sub>O<sub>x</sub> < Co<sub>7</sub>Mn<sub>3</sub>O<sub>x</sub>, and the apparent energy barrier of Co<sub>3</sub>Mn<sub>7</sub>O<sub>x</sub> (19.3 kJ/mol), Co<sub>5</sub>Mn<sub>5</sub>O<sub>x</sub> (18.8 kJ/mol) and Co<sub>7</sub>Mn<sub>3</sub>O<sub>x</sub> (15.7 kJ/mol) are significantly lower than that of MnO<sub>x</sub> (33.9 kJ/mol) and CoO<sub>x</sub> (24.3 kJ/mol). These results showed that the energy barrier of MnO<sub>x</sub> and CoO<sub>x</sub> was greatly changed after a second element was introduced, meaning that the active sites formed on these catalysts may be altered.

Meanwhile, the effect of calcination temperature of MnO<sub>x</sub> and Co<sub>7</sub>Mn<sub>3</sub>O<sub>x</sub> catalysts on their NH<sub>3</sub>-SCR activity was also detected. As shown in Fig. 3, when increasing the calcination temperature of MnO<sub>x</sub> from 450 to 650 °C, the highest NO<sub>x</sub> conversion decreased from 97% over MnO<sub>x</sub>-450 to 27% over MnO<sub>x</sub>-650. Although the NH<sub>3</sub>-SCR activity of the Co<sub>7</sub>Mn<sub>3</sub>O<sub>x</sub> catalyst also decreased when increasing the calcination temperature, more than 80% NO<sub>x</sub> can be removed in the operation temperature window ranged from 160 to 254 °C over the Co<sub>7</sub>Mn<sub>3</sub>O<sub>x</sub>-650 catalyst. This results indicated that the Co<sub>7</sub>Mn<sub>3</sub>O<sub>x</sub> catalyst exhibited a higher thermal stability in the NH<sub>3</sub>-SCR reaction compared

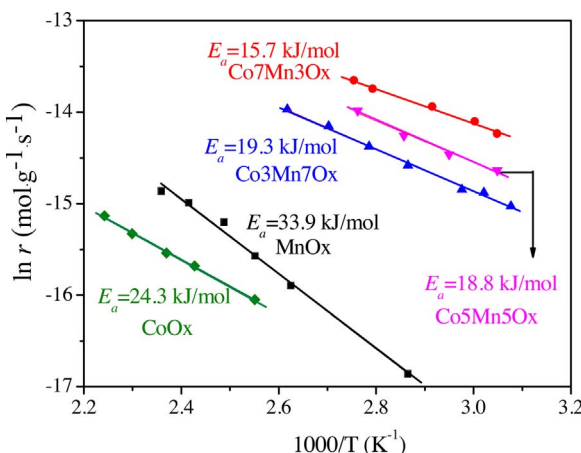


Fig. 2. Arrhenius plot for the NH<sub>3</sub>-SCR over the MnO<sub>x</sub>-550, CoO<sub>x</sub>-550 and Co<sub>a</sub>Mn<sub>b</sub>O<sub>x</sub>-550 catalysts.

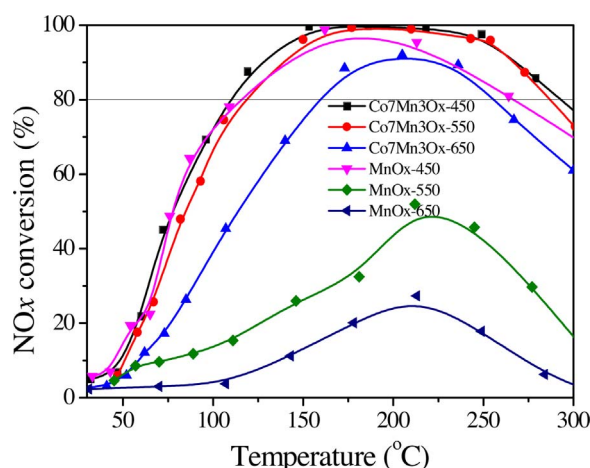


Fig. 3. NO<sub>x</sub> conversion as a function of temperature in the NH<sub>3</sub>-SCR reaction over the Co<sub>7</sub>Mn<sub>3</sub>O<sub>x</sub> and MnO<sub>x</sub> catalysts calcined at different temperature. (Reaction conditions: 0.3 g of sample, 500 ppm NO + 500 ppm NH<sub>3</sub> + 5 vol.% H<sub>2</sub>O + 5 vol.% O<sub>2</sub>/Ar balanced, total flow rate 300 mL/min and GHSV = 80000 h<sup>-1</sup>).

with MnO<sub>x</sub>, which has a beneficial effect on the practical application of the Co<sub>7</sub>Mn<sub>3</sub>O<sub>x</sub> catalyst.

On the other hand, to emphasize the advantages of the prepared catalysts, a series of catalysts for industrial applications, such as vanadium based catalysts and Cu-based zeolites, were considered as benchmark catalysts to compare the NH<sub>3</sub>-SCR activity, and their activity is directly extracted from the references. As shown in Fig. S1, the prepared Co<sub>a</sub>Mn<sub>b</sub>O<sub>x</sub> catalysts behaved a high NH<sub>3</sub>-SCR activity at low temperature and under a high space velocity, while vanadium based catalysts and Cu-based zeolites exhibited a wider temperature window for NO<sub>x</sub> removal. Furthermore, the Co<sub>7</sub>Mn<sub>3</sub>O<sub>x</sub>-550 catalyst exhibited a wider temperature window for NO<sub>x</sub> removal at the low temperature, compared with those reported Mn-based catalysts, as shown in Fig. S2.

### 3.2. Effect of SO<sub>2</sub> on the SCR reaction

As required for the practical use of NH<sub>3</sub>-SCR catalysts, water and SO<sub>2</sub> inevitably exist in the tail gas of power stations, which may quickly poison the catalyst. Fig. 4 displays the effect of H<sub>2</sub>O and SO<sub>2</sub> on the activity of the MnO<sub>x</sub>, Co<sub>3</sub>Mn<sub>7</sub>O<sub>x</sub> and Co<sub>7</sub>Mn<sub>3</sub>O<sub>x</sub> catalysts for the SCR reaction. The catalyst was kept under the reaction conditions for 4 h, and then 5 vol.% H<sub>2</sub>O was introduced into the feed gas mixture for 8 h. After that, the reaction gas atmosphere was reset to ideal conditions for 2 h, followed by a reaction atmosphere including 50 ppm SO<sub>2</sub>. As

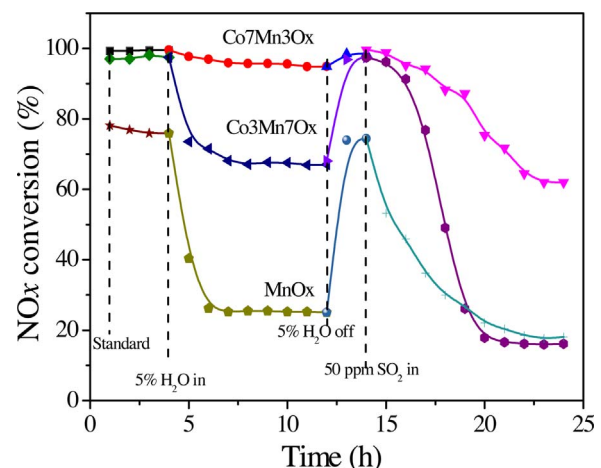


Fig. 4. Effect of water and SO<sub>2</sub> on the catalytic activities of the MnO<sub>x</sub>, Co<sub>3</sub>Mn<sub>7</sub>O<sub>x</sub> and Co<sub>7</sub>Mn<sub>3</sub>O<sub>x</sub> catalysts for the SCR reaction. (Reaction conditions: 0.3 g sample; 180 °C; 500 ppm NO + 500 ppm NH<sub>3</sub> + 5 vol.% O<sub>2</sub> + 5 vol.% H<sub>2</sub>O (when used) + 50 ppm SO<sub>2</sub> (when used)/Ar balanced, total flow rate 300 mL/min and GHSV = 80000 h<sup>-1</sup>).

shown in Fig. 4, when 5 vol.% H<sub>2</sub>O is introduced into the feed gas, NO<sub>x</sub> conversion decreases drastically to 25% and 67% over the MnO<sub>x</sub> and Co<sub>3</sub>Mn<sub>7</sub>O<sub>x</sub> catalysts, respectively. However, NO<sub>x</sub> conversion remains greater than 95% over the Co<sub>7</sub>Mn<sub>3</sub>O<sub>x</sub> catalyst during the same period, indicating that the Co<sub>7</sub>Mn<sub>3</sub>O<sub>x</sub> catalyst possesses excellent water-resistance performance. At the same time, the Co<sub>7</sub>Mn<sub>3</sub>O<sub>x</sub> catalyst exhibits excellent sulfur-resistance performance. The high activity with 62% NO<sub>x</sub> conversion can be maintained over the Co<sub>7</sub>Mn<sub>3</sub>O<sub>x</sub> catalyst after poisoning by the feed gas that includes 50 ppm SO<sub>2</sub> for 10 h, whereas the other two samples are almost deactivated completely. Furthermore, even if 5% H<sub>2</sub>O and 50 ppm SO<sub>2</sub> were introduced into the feed gas simultaneously, NO<sub>x</sub> conversion over the Co<sub>7</sub>Mn<sub>3</sub>O<sub>x</sub> catalyst is also much higher than that over the other two samples (Fig. S3), confirming a high water-resistance and sulfur-resistance performance of the Co<sub>7</sub>Mn<sub>3</sub>O<sub>x</sub> catalyst. On the other hand, it is interesting that all the MnO<sub>x</sub>, Co<sub>3</sub>Mn<sub>7</sub>O<sub>x</sub> and Co<sub>7</sub>Mn<sub>3</sub>O<sub>x</sub> catalysts can be regenerated simply by washing with water. As shown in Fig. 5, the catalytic activities of the catalysts can be recovered, and even the activities of the MnO<sub>x</sub> and Co<sub>3</sub>Mn<sub>7</sub>O<sub>x</sub> catalysts are better than those of the fresh samples. As a result, regenerated Co<sub>3</sub>Mn<sub>7</sub>O<sub>x</sub> and Co<sub>7</sub>Mn<sub>3</sub>O<sub>x</sub> catalysts show the similar SCR activity. The reason for the decreased gap between the SCR activity of regenerated Co<sub>3</sub>Mn<sub>7</sub>O<sub>x</sub> and Co<sub>7</sub>Mn<sub>3</sub>O<sub>x</sub> catalysts compared with fresh

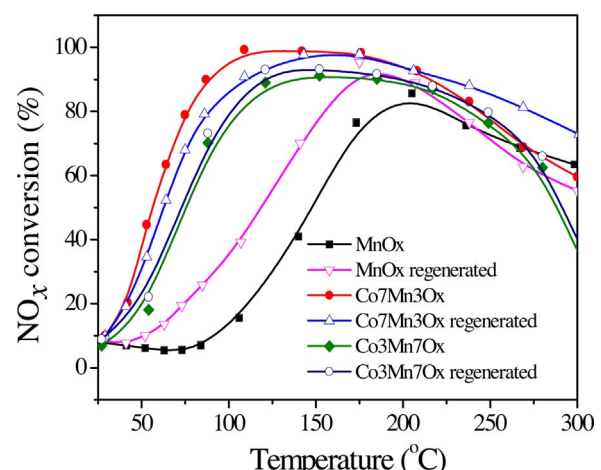


Fig. 5. Catalytic activities of the fresh and regenerated MnO<sub>x</sub>, Co<sub>3</sub>Mn<sub>7</sub>O<sub>x</sub> and Co<sub>7</sub>Mn<sub>3</sub>O<sub>x</sub> catalysts for the SCR reaction. (Reaction conditions: 0.3 g of sample, 500 ppm NO + 500 ppm NH<sub>3</sub> + 5 vol.% O<sub>2</sub>/Ar balanced, total flow rate 300 mL/min and GHSV = 80000 h<sup>-1</sup>).

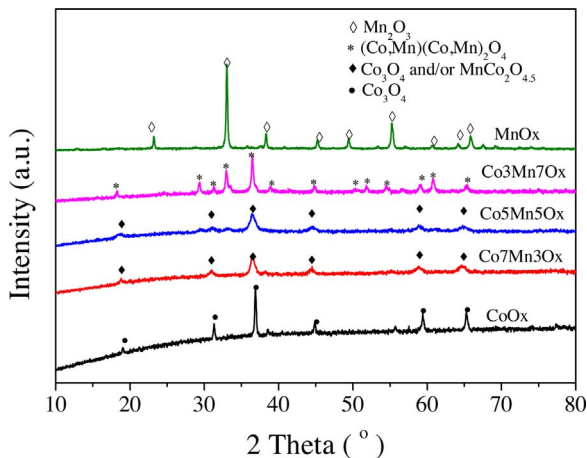


Fig. 6. XRD patterns of the  $\text{Co}_a\text{Mn}_b\text{O}_x$  catalysts with different Co/Mn mole ratio.

catalysts may be the decrease in their activity for NO oxidation, which makes the catalytic activity of two catalysts for NO oxidation closer (Fig. S4).

### 3.3. Structural properties of the catalysts

Fig. 6 depicts the XRD patterns of the  $\text{CoO}_x$ ,  $\text{MnO}_x$  and  $\text{Co}_a\text{Mn}_b\text{O}_x$  catalysts with various Co/Mn molar ratios. In the XRD patterns of  $\text{CoO}_x$  and  $\text{MnO}_x$ , the diffraction peaks mainly represent spinel structured  $\text{Co}_3\text{O}_4$  and  $\text{Mn}_2\text{O}_3$ , respectively. The XRD patterns of the  $\text{Co}_a\text{Mn}_b\text{O}_x$  catalysts vary with the Co/Mn molar ratio. The  $\text{Co}_3\text{Mn}_7\text{O}_x$  catalyst presents diffraction peaks for well crystallized  $(\text{Co}, \text{Mn})(\text{Co}, \text{Mn})_2\text{O}_4$ , and the diffraction peaks of  $\text{MnCo}_2\text{O}_{4.5}$  or  $\text{Co}_3\text{O}_4$  are shown in the XRD patterns of the  $\text{Co}_5\text{Mn}_5\text{O}_x$  and  $\text{Co}_7\text{Mn}_3\text{O}_x$  catalysts [21,22]. Since the diffraction peaks of  $\text{Co}_3\text{O}_4$  and  $\text{MnCo}_2\text{O}_{4.5}$  are present at very similar  $2\theta$  angles and the Co/Mn molar ratio of the  $\text{Co}_7\text{Mn}_3\text{O}_x$  catalyst is higher than that of  $\text{MnCo}_2\text{O}_{4.5}$ , it is deduced that the diffraction peaks in the XRD pattern of the  $\text{Co}_7\text{Mn}_3\text{O}_x$  catalyst may overlap with the signals of  $\text{Co}_3\text{O}_4$  and  $\text{MnCo}_2\text{O}_{4.5}$ . In contrast, the Co/Mn molar ratio of the  $\text{Co}_5\text{Mn}_5\text{O}_x$  catalyst is lower than that of  $\text{MnCo}_2\text{O}_{4.5}$ , and the diffraction peaks of  $\text{Mn}_2\text{O}_3$  do not appear in the XRD patterns of the  $\text{Co}_5\text{Mn}_5\text{O}_x$  catalyst, indicating that some of the  $\text{MnO}_x$  may be homogeneously dispersed on the catalyst surface with the other species.

The Raman spectra of the catalysts are shown in Fig. 7. There are five peaks centered at 190, 466, 509, 605 and  $674 \text{ cm}^{-1}$  for the  $\text{CoO}_x$  catalyst, which are assigned to the  $\text{F}_{2g}$ ,  $\text{E}_g$ ,  $\text{F}_{2g}$ ,  $\text{F}_{2g}$  and  $\text{A}_{1g}$  symmetries, respectively [23,24]. For the  $\text{MnO}_x$  catalyst, only a strong peak at  $635 \text{ cm}^{-1}$  existed, which was assigned to  $\text{Mn}_2\text{O}_3$  with a distorted

hausmannite structure [25–28]. The Raman spectra of the  $\text{Co}_a\text{Mn}_b\text{O}_x$  catalysts are greatly different from those of  $\text{CoO}_x$  and  $\text{MnO}_x$  and depend on the molar ratio of Co/Mn in the catalysts. There are two strong peaks at 605 and  $650 \text{ cm}^{-1}$  assigned to  $\text{MnO}_2$  and  $\text{Mn}_3\text{O}_4$  species, respectively, in the Raman spectra of the  $\text{Co}_3\text{Mn}_7\text{O}_x$  catalyst [28–30]. In contrast, the  $\text{Co}_7\text{Mn}_3\text{O}_x$  catalyst exhibits two strong peaks at 605 and  $674 \text{ cm}^{-1}$  assigned to  $\text{MnO}_2$  and  $\text{Co}_3\text{O}_4$  species, respectively. The presence of  $\text{Co}_3\text{O}_4$  in the  $\text{Co}_7\text{Mn}_3\text{O}_x$  catalyst is also reflected in the XRD profiles. Finally, the lower Raman signal intensity of the cobalt-containing samples indicated the reduced crystallinity of these catalysts [31], which is consistent with the XRD results.

TEM images of the  $\text{MnO}_x$ ,  $\text{CoO}_x$ ,  $\text{Co}_3\text{Mn}_7\text{O}_x$  and  $\text{Co}_7\text{Mn}_3\text{O}_x$  catalysts are displayed in Fig. 8. The four samples exhibited similar irregular particles, and their sizes are ranked in the order of  $\text{MnO}_x > \text{CoO}_x > \text{Co}_3\text{Mn}_7\text{O}_x > \text{Co}_7\text{Mn}_3\text{O}_x$ . The sizes of the  $\text{Co}_3\text{O}_4$  particles are mainly 30–80 nm, and the lattice spacing is 0.475 nm, which is assigned to the  $\text{Co}_3\text{O}_4$  (111) facet. The  $\text{MnO}_x$  catalyst consisted of nanoparticles and nanorods, and the nanorods resulted from the adhesion or agglomeration of nanoparticles. The lattice spacings are 0.396 nm, 0.315 nm and 0.250 nm, which correspond to the  $\text{Mn}_2\text{O}_3$  (211), (122) and (321) facets. However, several types of stripes are present on the  $\text{Co}_3\text{Mn}_7\text{O}_x$  catalyst (Fig. 8C). Those with lattice spacings of 0.503 nm and 0.272 nm are ascribed to the  $(\text{Co}, \text{Mn})(\text{Co}, \text{Mn})_2\text{O}_4$  (111) and (113) facets, and the lattice spacing of 0.390 nm is probably ascribed to the (211) facet of excess  $\text{Mn}_2\text{O}_3$  that was formed. For the  $\text{Co}_7\text{Mn}_3\text{O}_x$  catalyst (Fig. 8D), the lattice spacings of 0.473 nm and 0.259 nm are attributed to the  $\text{MnCo}_2\text{O}_4$  (111) and (311) facets. Compared with the particle size of  $\text{Co}_3\text{Mn}_7\text{O}_x$  (15–50 nm), the  $\text{Co}_7\text{Mn}_3\text{O}_x$  catalyst exhibited a smaller size (6–30 nm), resulting in a larger specific surface area (Table 1).

Fig. 9 shows the O 1s, Co 2p and Mn 2p XPS spectra of the  $\text{MnO}_x$ ,  $\text{CoO}_x$ ,  $\text{Co}_3\text{Mn}_7\text{O}_x$ ,  $\text{Co}_5\text{Mn}_5\text{O}_x$  and  $\text{Co}_7\text{Mn}_3\text{O}_x$  catalysts. In the O 1s XPS spectra, all catalysts exhibited two distinguishing peaks. The peak at B.E. = 529.0–529.8 eV is attributed to lattice oxygen ( $\text{O}_L$ ), and the peak at 530.5–531.3 eV belongs to surface oxygen ( $\text{O}_S$ ), including surface adsorbed oxygen (such as  $\text{O}_2^-$  or  $\text{O}^-$ ) and that of hydroxyl-like groups [32]. The  $\text{OS}/(\text{OS} + \text{OL})$  ratios of the catalysts were calculated and are shown in Table 1. The ratios of  $\text{O}_S/(\text{O}_L + \text{O}_S)$  for the  $\text{Co}_7\text{Mn}_3\text{O}_x$ ,  $\text{Co}_5\text{Mn}_5\text{O}_x$ ,  $\text{Co}_3\text{Mn}_7\text{O}_x$  and  $\text{MnO}_x$  catalysts are 32%, 33%, 43% and 42%, respectively, which is much lower than that of the  $\text{CoO}_x$  (63%) catalyst. In the Co 2p XPS spectra, the peaks at  $779.4 \pm 0.3 \text{ eV}$  and  $780.8 \pm 0.1 \text{ eV}$  are assigned to  $\text{Co}^{3+}$  and  $\text{Co}^{2+}$ , respectively [33]. The peak at  $786.3 \pm 0.1 \text{ eV}$  is the satellite peak of Co 2p. As shown in Table 1, the  $\text{Co}^{3+}/(\text{Co}^{2+} + \text{Co}^{3+})$  ratios for the  $\text{Co}_7\text{Mn}_3\text{O}_x$ ,  $\text{Co}_5\text{Mn}_5\text{O}_x$  and  $\text{Co}_3\text{Mn}_7\text{O}_x$  catalysts are 42.6%, 56.2% and 44.3%, respectively, which is lower than that of the  $\text{CoO}_x$  catalyst (73.8%). In the Mn 2p XPS spectra, three peaks can be observed at 635–647 eV for all the catalysts. The peaks at  $640.1 \pm 0.4$  and  $641.6 \pm 0.2 \text{ eV}$  represent  $\text{Mn}^{3+}$  and  $\text{Mn}^{4+}$ , respectively [34], and the peak at  $643.5 \pm 0.3 \text{ eV}$  is assigned to the satellite peak of Mn 2p [35]. As shown in Table 1, the atomic ratio of  $\text{Mn}^{4+}/(\text{Mn}^{3+} + \text{Mn}^{4+})$  in the  $\text{Co}_7\text{Mn}_3\text{O}_x$  catalyst was 76.4%, which is much higher than that in the  $\text{MnO}_x$  (25.3%),  $\text{Co}_3\text{Mn}_7\text{O}_x$  (64.4%) and  $\text{Co}_5\text{Mn}_5\text{O}_x$  (53.4%) catalysts, probably due to the different  $\text{MnCoO}_x$  phases formed between the  $\text{Co}_3\text{Mn}_7\text{O}_x$ ,  $\text{Co}_5\text{Mn}_5\text{O}_x$  and  $\text{Co}_7\text{Mn}_3\text{O}_x$  catalysts. As is well known, high concentrations of surface oxygen ( $\text{O}_S$ ) and metal ions with high oxidation states (such as  $\text{Mn}^{4+}$  and  $\text{Co}^{3+}$ ) on the catalyst surface are beneficial to the catalytic oxidation ability of this catalyst, which can enhance the oxidation of NO to  $\text{NO}_2$  to accelerate the  $\text{NH}_3\text{-SCR}$  reaction. Based on the XPS results, it is impossible to directly estimate or compare the oxidation ability of the  $\text{MnO}_x$ ,  $\text{Co}_3\text{Mn}_7\text{O}_x$ ,  $\text{Co}_5\text{Mn}_5\text{O}_x$  and  $\text{Co}_7\text{Mn}_3\text{O}_x$  catalysts because the changes in the parameters in relation to their oxidation ability are not uniform.

### 3.4. Reducibility and oxidizability of the catalysts

Fig. 10 shows the  $\text{H}_2\text{-TPR}$  profiles of the  $\text{CoO}_x$ ,  $\text{MnO}_x$  and  $\text{Co}_a\text{Mn}_b\text{O}_x$

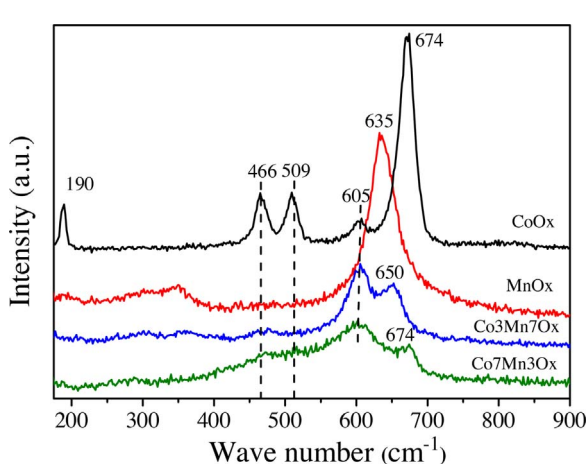


Fig. 7. Raman spectra of the  $\text{CoO}_x$ ,  $\text{MnO}_x$  and  $\text{Co}_a\text{Mn}_b\text{O}_x$  catalysts.

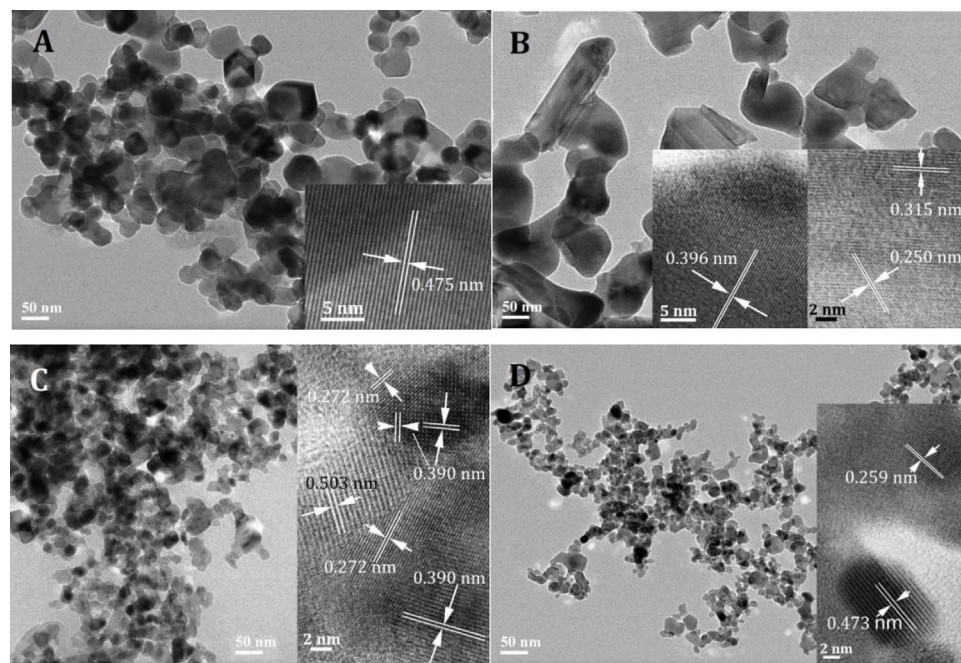


Fig. 8. TEM images of the  $\text{CoO}_x$  (A),  $\text{MnO}_x$  (B),  $\text{Co}_3\text{Mn}_7\text{O}_x$  (C) and  $\text{Co}_7\text{Mn}_3\text{O}_x$  (D) catalysts.

catalysts. The  $\text{CoO}_x$  catalyst exhibits two reduction peaks at 315 and 393 °C, which are ascribed to the reduction of  $\text{Co}^{3+} \rightarrow \text{Co}^{2+}$  and  $\text{Co}^{2+} \rightarrow \text{Co}$ , respectively [36]. The  $\text{MnO}_x$  catalyst exhibits two reduction peaks at 346 and 441 °C, belonging to the reduction of  $\text{MnO}_2/\text{Mn}_2\text{O}_3 \rightarrow \text{Mn}_3\text{O}_4$  and  $\text{Mn}_3\text{O}_4 \rightarrow \text{MnO}$ , respectively [15,21,37–41,42]. However, three reduction peaks appeared in the  $\text{H}_2\text{-TPR}$  profiles of all of the  $\text{Co}_a\text{Mn}_b\text{O}_x$  catalysts. The  $\alpha$  peak at 259–269 °C is ascribed to the reduction of  $\text{MnO}_2$  to  $\text{Mn}_2\text{O}_3$  [17,43], and the amount of  $\text{H}_2$  consumption for the  $\text{Co}_3\text{Mn}_7\text{O}_x$  catalyst is higher than that for the  $\text{Co}_7\text{Mn}_3\text{O}_x$  and  $\text{Co}_5\text{Mn}_5\text{O}_x$  catalysts, due to the higher amount of  $\text{Mn}^{4+}$  on the  $\text{Co}_3\text{Mn}_7\text{O}_x$  surface. As shown in Table 1, although the atomic ratio of  $\text{Mn}^{4+}/(\text{Mn}^{3+} + \text{Mn}^{4+})$  on the  $\text{Co}_3\text{Mn}_7\text{O}_x$  surface is slightly lower than that on the  $\text{Co}_7\text{Mn}_3\text{O}_x$  catalyst, the Mn content in the  $\text{Co}_3\text{Mn}_7\text{O}_x$  catalyst is much higher than that in the  $\text{Co}_7\text{Mn}_3\text{O}_x$  catalyst, resulting in more  $\text{Mn}^{4+}$  on the  $\text{Co}_3\text{Mn}_7\text{O}_x$  surface. The  $\beta$  peak at 332–368 °C is assigned to the simultaneous reduction of  $\text{Co}^{3+} \rightarrow \text{Co}^{2+}$  and  $\text{Mn}_2\text{O}_3 \rightarrow \text{Mn}_3\text{O}_4$ , and the  $\gamma$  peak at 493 °C is assigned to the reduction of  $\text{Co}^{2+} \rightarrow \text{Co}$  and  $\text{Mn}_3\text{O}_4 \rightarrow \text{MnO}$ . For the  $\text{Co}_3\text{Mn}_7\text{O}_x$ ,  $\text{Co}_5\text{Mn}_5\text{O}_x$  and  $\text{Co}_7\text{Mn}_3\text{O}_x$  catalysts, the amount of  $\text{H}_2$  consumption for the  $\beta$  peak is similar. However, the amount of  $\text{H}_2$  consumption for the  $\gamma$  peak increased with increasing the Co amount in the  $\text{Co}_a\text{Mn}_b\text{O}_x$  catalysts. On the other hand, the highest temperatures of  $\alpha$  and  $\beta$  peaks for the  $\text{Co}_7\text{Mn}_3\text{O}_x$  catalyst are slightly lower than those for other two catalysts. In summary, the  $\text{Co}_3\text{Mn}_7\text{O}_x$ ,  $\text{Co}_5\text{Mn}_5\text{O}_x$  and  $\text{Co}_7\text{Mn}_3\text{O}_x$  catalysts exhibit similar reducibility at low temperature (< 400 °C), but their reducibility is much better than those of the  $\text{MnO}_x$  and  $\text{CoO}_x$  catalysts.

The oxidation abilities of the catalysts were investigated by both the CO oxidation and  $\text{O}_2\text{-TPD}$  techniques. The CO +  $\text{O}_2$  reaction on the  $\text{CoO}_x$ ,  $\text{MnO}_x$  and  $\text{Co}_a\text{Mn}_b\text{O}_x$  catalysts was estimated and is shown in Fig. 11a. All of the  $\text{CoO}_x$ ,  $\text{MnO}_x$ ,  $\text{Co}_3\text{Mn}_7\text{O}_x$  and  $\text{Co}_7\text{Mn}_3\text{O}_x$  catalysts exhibited similar high catalytic activity, indicating that all of the catalysts showed similar oxidizability under CO oxidation conditions. In the  $\text{O}_2\text{-TPD-MS}$  profiles (Fig. 11b), the desorption peaks below 250 °C can be ascribed to surface adsorbed oxygen, including  $\text{O}_2^-$  and  $\text{O}^-$ . Above this temperature, desorbed O species are attributed to lattice oxygen. In comparison with the catalysts containing low Mn amounts ( $\text{CoO}_x$  and  $\text{Co}_7\text{Mn}_3\text{O}_x$ ), the catalysts containing high Mn amounts ( $\text{Co}_3\text{Mn}_7\text{O}_x$  and  $\text{MnO}_x$ ) have much more mobile lattice oxygen at > 250 °C.

To further investigate the reactivity and recovery of the lattice oxygen of the catalyst, alternating experiments of CO reduction and  $\text{O}_2$  re-oxidation over the catalysts were run at 250 °C (the surface adsorbed oxygen can be removed at this temperature according to  $\text{O}_2\text{-TPD}$ ). As shown in Fig. 12, for the  $\text{MnO}_x$  catalyst, the formed  $\text{CO}_2$  signal is the largest in the first CO reduction cycle; after the sample was re-oxidized for 5 min, the signal of the formed  $\text{CO}_2$  decreased greatly in the second cycle, and CO was introduced; in the following repeated test of CO reduction- $\text{O}_2$  re-oxidation, similar results to the second run were obtained. This shows that a number of the lattice oxygen in  $\text{MnO}_x$  that were reduced by CO could not be recovered to their initial state in the fresh sample. Unlike the  $\text{MnO}_x$  sample, the first signal of formed  $\text{CO}_2$  is almost the same as the subsequent  $\text{CO}_2$  signals in  $\text{Co}_7\text{Mn}_3\text{O}_x$ , which means that the lattice oxygen consumed by CO reduction can be

Table 1  
BET surface area ( $S_{\text{BET}}$ ) and surface composition of  $\text{Co}_a\text{Mn}_b\text{O}_x$  with different Co/Mn molar ratios.

Catalyst	$S_{\text{BET}}$ ( $\text{m}^2/\text{g}$ )	Co/Mn (mol)		$\text{Co}^{3+} / (\text{Co}^{2+} + \text{Co}^{3+})^b$ (%)	$\text{O}_s / (\text{O}_l + \text{O}_s)^b$ (%)	$\text{Mn}^{4+} / (\text{Mn}^{4+} + \text{Mn}^{3+})^b$ (%)
		In bulk <sup>a</sup>	On surface <sup>b</sup>			
$\text{MnO}_x$	18	–	–	–	42	25.3
$\text{Co}_3\text{Mn}_7\text{O}_x$	20	0.44	0.26	44.3	43	64.4
$\text{Co}_5\text{Mn}_5\text{O}_x$	55	0.82	0.75	56.2	33	53.4
$\text{Co}_7\text{Mn}_3\text{O}_x$	51	2.33	2.29	42.6	32	76.4
$\text{CoO}_x$	10	–	–	73.8	63	–

<sup>a</sup> Determined by the ICP analysis.

<sup>b</sup> Calculated by the XPS data.

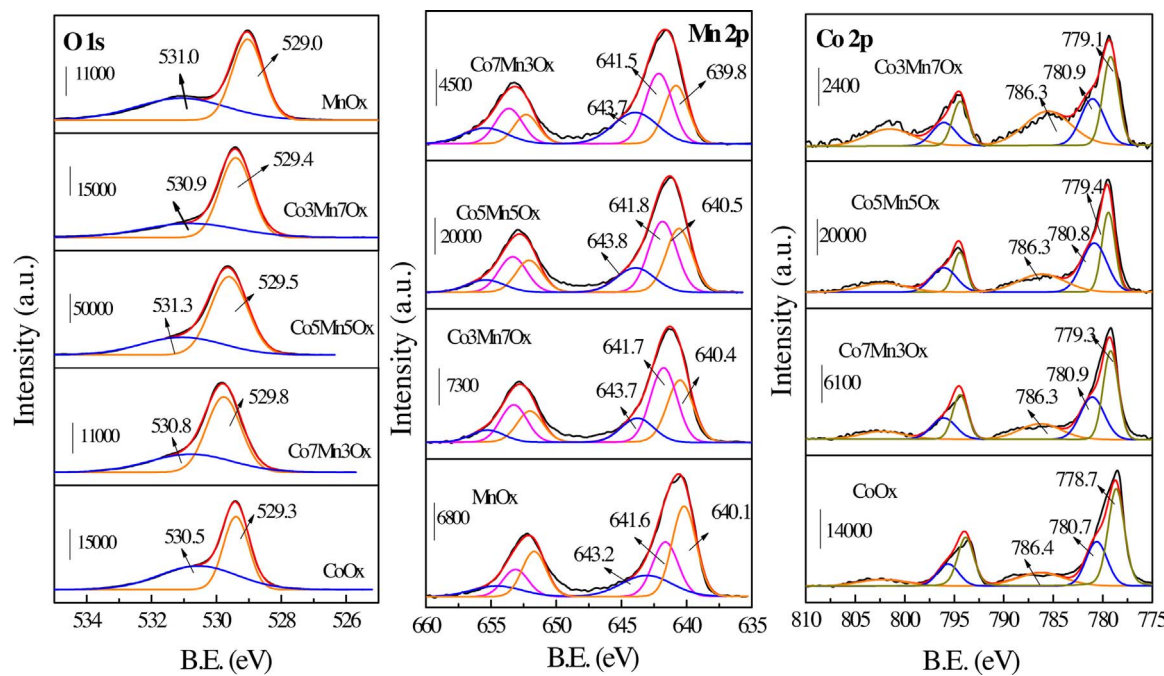


Fig. 9. O1s, Co 2p and Mn 2p XPS spectra of the  $\text{MnO}_x$ ,  $\text{C}_3\text{Mn}_7\text{O}_x$ ,  $\text{C}_5\text{Mn}_5\text{O}_x$ ,  $\text{Co}_7\text{Mn}_3\text{O}_x$  and  $\text{CoO}_x$  catalysts.

recovered after 5 min of re-oxidation with gaseous oxygen. The results above show that  $\text{Co}_7\text{Mn}_3\text{O}_x$  has better oxygen mobility than  $\text{MnO}_x$ , and consumed lattice oxygen can be quickly replenished by gaseous oxygen.

The ability for  $\text{NH}_3$  adsorption is one of the deciding factors for  $\text{NH}_3$ -SCR catalysts, thus the surface acidity of the catalyst is important for an excellent  $\text{NH}_3$ -SCR catalyst. The  $\text{NH}_3$ -TPD profiles of the  $\text{CoO}_x$ ,  $\text{MnO}_x$  and  $\text{Co}_a\text{Mn}_b\text{O}_x$  catalysts are shown in Fig. 13. In the  $\text{NH}_3$ -TPD profile of  $\text{MnO}_x$  there are mainly two overlapped desorption peaks at 80 and 180 °C, and for the  $\text{CoO}_x$  catalyst, three overlapped desorption peaks centered at 102, 180 and 315 °C can be observed. For the  $\text{Co}_a\text{Mn}_b\text{O}_x$  catalysts, desorption peaks similar to those of the  $\text{CoO}_x$  and  $\text{MnO}_x$  catalysts can be observed, but their intensities are obviously improved by increasing the molar ratio of Co/Mn, where the  $\text{Co}_7\text{Mn}_3\text{O}_x$  catalyst possessed the highest amount of acid sites among all  $\text{Co}_a\text{Mn}_b\text{O}_x$  catalysts. For the  $\text{NH}_3$ -SCR reaction, whether the mechanism is Langmuir-Hinshelwood or Eley-Rideal, the increase in the amount of surface acid sites can enhance the adsorption of  $\text{NH}_3$  and result in the

improvement of the  $\text{NH}_3$ -SCR reaction [32,44]. Therefore, the high  $\text{NH}_3$  adsorption ability of the  $\text{Co}_7\text{Mn}_3\text{O}_x$  catalyst is beneficial to its high catalytic activity in  $\text{NH}_3$ -SCR.

Since the  $\text{NH}_3$  adsorption amount may be affected by the surface area of the catalyst and  $\text{NH}_3$  desorbing below 250 °C is considered effective for low-temperature  $\text{NH}_3$ -SCR, the integrated areas of the desorption peaks at < 250 °C per unit surface area ( $\text{Area}/S_{\text{BET}}$ , a.u./ $\text{m}^2$ ) were calculated. The  $\text{Area}/S_{\text{BET}}$  values ranked as follows:  $\text{CoO}_x$  (84.3) >  $\text{Co}_3\text{Mn}_7\text{O}_x$  (66.4) >  $\text{Co}_7\text{Mn}_3\text{O}_x$  (53.3) >  $\text{MnO}_x$  (41.3). The abovementioned results showed that the  $\text{CoO}_x$  catalyst exhibited stronger acidic properties and had more acidic sites at < 250 °C than the  $\text{MnO}_x$  catalyst. This means that the presence of Co in the  $\text{Co}_a\text{Mn}_b\text{O}_x$  catalyst can increase the acidic properties and the  $\text{NH}_3$  adsorption ability of  $\text{MnO}_x$ . For the  $\text{Co}_7\text{Mn}_3\text{O}_x$  catalyst, because its surface area is the largest among all catalysts and even 5 times greater than that of the  $\text{CoO}_x$  catalyst, it has the most acid sites among all the catalysts.

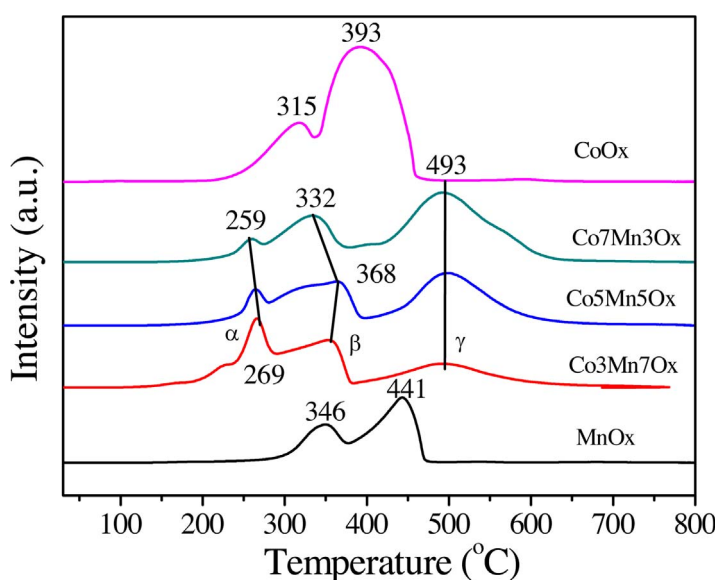


Fig. 10.  $\text{H}_2$ -TPR profiles of the  $\text{CoO}_x$ ,  $\text{MnO}_x$  and  $\text{Co}_a\text{Mn}_b\text{O}_x$  catalysts.

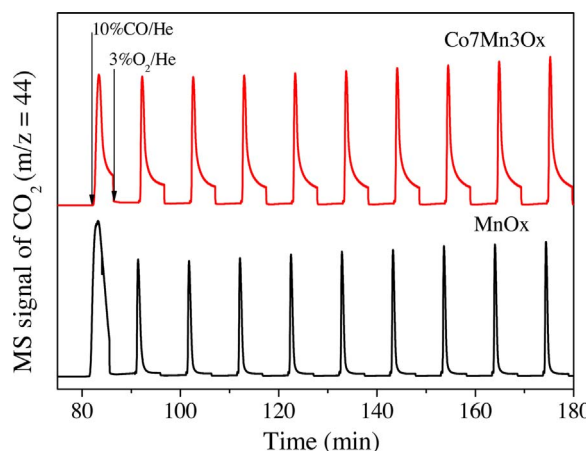
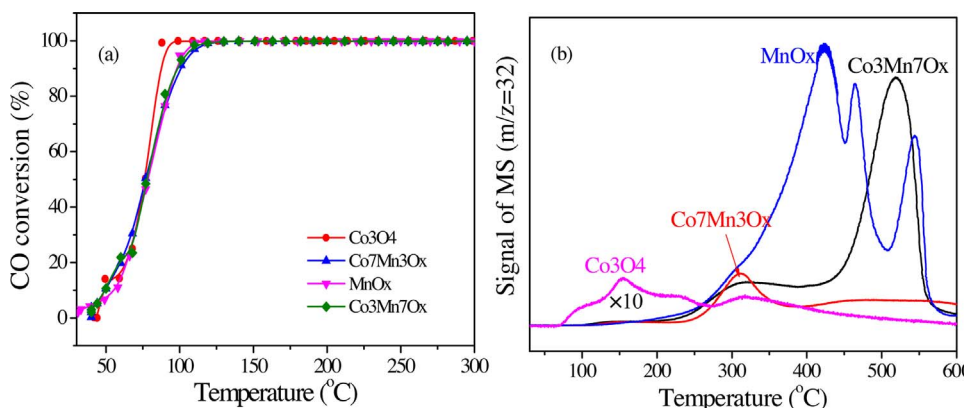


Fig. 12. Alternation experiments of CO reduction and O<sub>2</sub> re-oxidation over the Co<sub>7</sub>Mn<sub>3</sub>O<sub>x</sub>-550 and MnO<sub>x</sub>-550 samples at 250 °C. (Reaction conditions: 50 mg sample pre-treated in He at 250 °C for 60 min, 10%CO/He was passed the catalyst bed for 5 min, then 3% O<sub>2</sub>/He was used to oxidize the catalyst for 5 min).

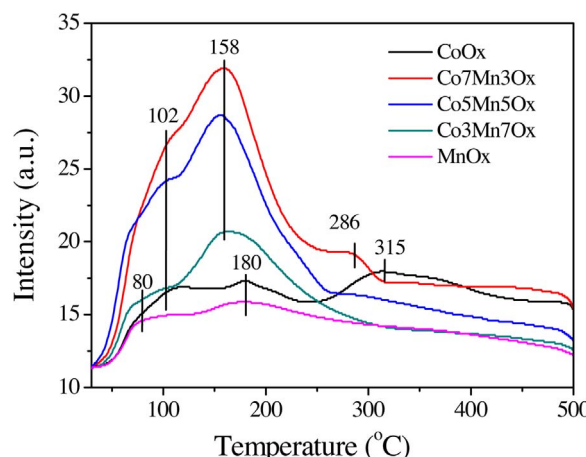


Fig. 13. NH<sub>3</sub>-TPD profiles of the CoO<sub>x</sub>, MnO<sub>x</sub> and Co<sub>a</sub>Mn<sub>b</sub>O<sub>x</sub> catalysts.

### 3.5. Catalytic activity for NO oxidation and adsorption ability for NO<sub>x</sub>

It has been reported that a good SCR catalyst usually exhibits higher catalytic performance for NO oxidation, which is beneficial to the “fast SCR” reaction,  $\text{NO} + \text{NO}_2 + 2\text{NH}_3 \rightarrow 2\text{N}_2 + 3\text{H}_2\text{O}$ . Therefore, the catalytic activities of the catalysts for NO oxidation were studied, as shown in Fig. 14. For NO oxidation at low temperature (< 200 °C), the Co<sub>a</sub>Mn<sub>b</sub>O<sub>x</sub> catalysts exhibited similar catalytic activities, which are higher than those of the MnO<sub>x</sub> and CoO<sub>x</sub> catalysts. As shown in the H<sub>2</sub>-

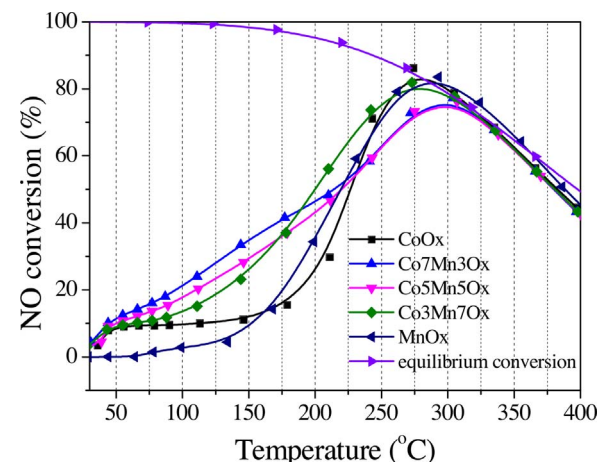


Fig. 14. NO oxidation over the CoO<sub>x</sub>, MnO<sub>x</sub> and Co<sub>a</sub>Mn<sub>b</sub>O<sub>x</sub> catalysts. (Reaction conditions: 500 ppm NO + 5 vol.% O<sub>2</sub>/Ar balanced, total flow rate 300 mL/min and GHSV = 80000 h<sup>-1</sup>).

TPR profiles, the Co<sub>a</sub>Mn<sub>b</sub>O<sub>x</sub> catalysts displayed similar reducibility at low temperature, which may be the reason for the similar activities of the Co<sub>a</sub>Mn<sub>b</sub>O<sub>x</sub> catalysts for NO oxidation. Comparing the catalytic performance for NO oxidation with the SCR activity (Fig. 1), no direct correspondence between their catalytic activities for NO oxidation and the NH<sub>3</sub>-SCR reaction can be observed. The reason may be that NO oxidation to NO<sub>2</sub> by oxygen is not the rate-determining step in the SCR reaction over these catalysts [11,45].

Fig. 15 shows the NO<sub>x</sub>-TPD profiles of the CoO<sub>x</sub>, MnO<sub>x</sub> and Co<sub>a</sub>Mn<sub>b</sub>O<sub>x</sub> catalysts after being treated in 500 ppm NO and 5% O<sub>2</sub>/Ar for 1 h with a flow rate of 300 mL/min. The shape of the entire curve changed significantly with the varied composition of the catalyst, due to the different surface phases of Co<sub>a</sub>Mn<sub>b</sub>O<sub>x</sub> in these catalysts. In the NO<sub>x</sub>-TPD curves of all catalysts except MnO<sub>x</sub>, there are three overlapped NO<sub>x</sub> desorption peaks in the temperature range of 50–400 °C. The desorption peak at < 200 °C is attributed to physisorbed NO<sub>x</sub> and decomposition of nitrite species, while the desorption peak at > 200 °C can be ascribed to the decomposition of bridged nitrate species and bidentate nitrate species with higher thermal stability [15,46–48]. Furthermore, the top temperatures of desorption peaks over the Co<sub>7</sub>Mn<sub>3</sub>O<sub>x</sub> catalyst are different from that over the Co<sub>3</sub>Mn<sub>7</sub>O<sub>x</sub> and Co<sub>5</sub>Mn<sub>5</sub>O<sub>x</sub> catalysts, due to the difference in the interaction between nitrate/nitrite species and the surface of the Co<sub>a</sub>Mn<sub>b</sub>O<sub>x</sub> catalysts composed with different MnO<sub>x</sub> phases.

On the other hand, the amount of desorbed NO<sub>x</sub> on the Co<sub>7</sub>Mn<sub>3</sub>O<sub>x</sub> catalyst is much more than that on the MnO<sub>x</sub>, CoO<sub>x</sub> and Co<sub>3</sub>Mn<sub>7</sub>O<sub>x</sub> catalysts and slightly more than that on the Co<sub>5</sub>Mn<sub>5</sub>O<sub>x</sub> catalyst. The integrated areas of desorption peak per square meter of surface area (Area/S<sub>BET</sub>) are calculated and their Area/S<sub>BET</sub> values are ranked in the

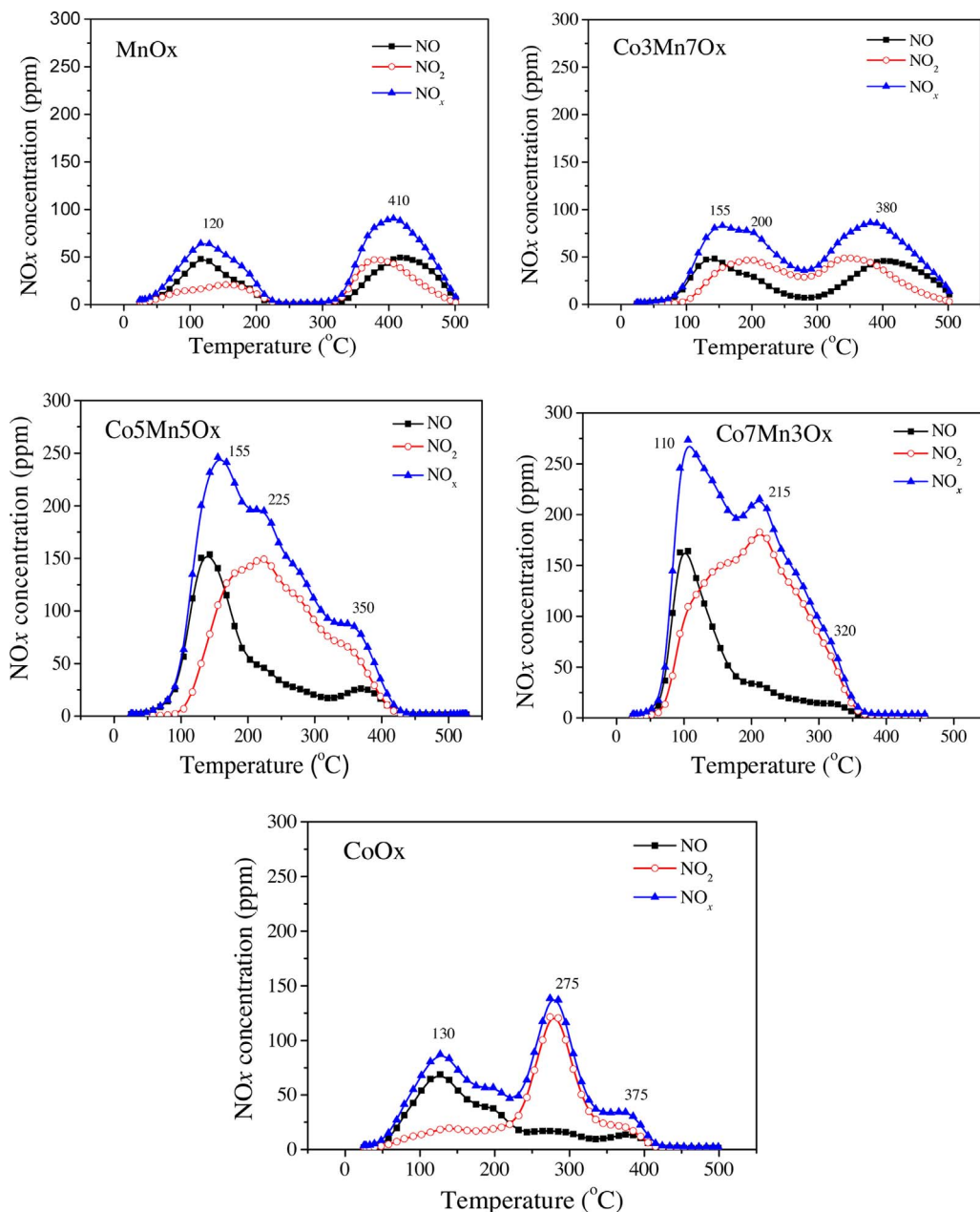


Fig. 15. NO<sub>x</sub>-TPD profiles of the CoO<sub>x</sub>, MnO<sub>x</sub> and Co<sub>a</sub>Mn<sub>b</sub>O<sub>x</sub> catalysts after being treated in 500 ppm NO/5% O<sub>2</sub>/Ar (300 mL/min) for 1 h.

order of CoO<sub>x</sub> (10.0  $\mu\text{mol}/\text{m}^2$ ) > Co<sub>3</sub>Mn<sub>7</sub>O<sub>x</sub> (5.5  $\mu\text{mol}/\text{m}^2$ ) > MnO<sub>x</sub> (4.4  $\mu\text{mol}/\text{m}^2$ )  $\approx$  Co<sub>7</sub>Mn<sub>3</sub>O<sub>x</sub> (4.2  $\mu\text{mol}/\text{m}^2$ ). This means that not only the specific surface area but also the Co<sub>a</sub>Mn<sub>b</sub>O<sub>x</sub> phases in the catalyst can influence the NO<sub>x</sub> adsorption ability of the catalyst.

### 3.6. In situ DRIFT spectroscopy

All catalysts were first pretreated in Ar (50 mL/min) at 300 °C for 2 h and then cooled to 50 °C. Subsequently, the catalyst was exposed to a gas mixture of 500 ppm NO + 5 vol.% O<sub>2</sub>/Ar (50 mL/min) at 50 °C, while in situ DRIFT spectra of the catalysts were taken at different times, and are shown in Fig. 16. There are many weak IR absorption bands at 1621, 1434, 1302 and 1215  $\text{cm}^{-1}$  in the spectrum of MnO<sub>x</sub> and absorption bands at 1458 and 1325  $\text{cm}^{-1}$  in the spectrum of CoO<sub>x</sub>. The absorption bands at 1621  $\text{cm}^{-1}$  can be attributed to bridged nitrates, and the absorption bands at 1325 and 1302  $\text{cm}^{-1}$  can be attributed to bidentate nitrates [49,50]. The band at 1215  $\text{cm}^{-1}$  indicates the existence of bridged nitrites [4,48,51], and the absorption bands at 1434 and 1458  $\text{cm}^{-1}$  belong to ionic nitrates [49]. After Co was added

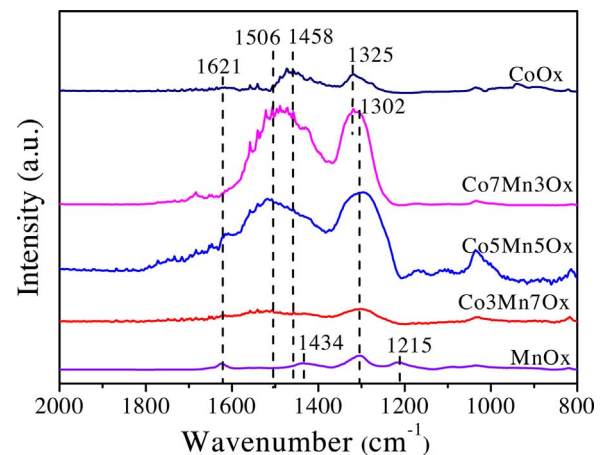


Fig. 16. In situ DRIFT spectra of the CoO<sub>x</sub>, MnO<sub>x</sub> and Co<sub>a</sub>Mn<sub>b</sub>O<sub>x</sub> catalysts in the mixed gas of 500 ppm NO + 5 vol.% O<sub>2</sub>/Ar (50 mL/min) at 50 °C for 60 min.

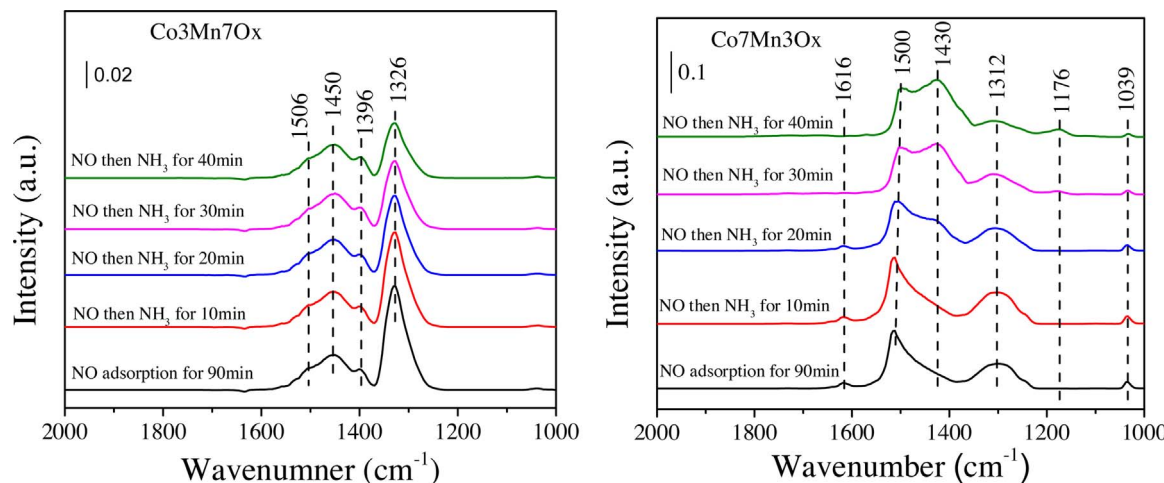


Fig. 17. In situ DRIFT spectra of the  $\text{Co}_3\text{Mn}_7\text{O}_x$  and  $\text{Co}_7\text{Mn}_3\text{O}_x$  catalysts in the mixed gas of 500 ppm  $\text{NH}_3/\text{Ar}$  for different times at 100 °C after adsorption of 500 ppm NO + 5 vol.%  $\text{O}_2/\text{Ar}$  at 100 °C for 90 min and blowing of Ar for 1 h.

into  $\text{MnO}_x$ , it can be seen that in situ DRIFT spectra of the  $\text{Co}_a\text{Mn}_b\text{O}_x$  catalysts were markedly influenced by the molar ratio of Co/Mn. The  $\text{Co}_3\text{Mn}_7\text{O}_x$  catalyst exhibits two very weak absorption bands at 1506 and 1302  $\text{cm}^{-1}$ , and the former absorption band is assigned to bidentate nitrate [52–54]. With increasing Co content, the intensity of the IR absorption bands greatly increased, as seen in the IR spectra of the  $\text{Co}_5\text{Mn}_5\text{O}_x$  and  $\text{Co}_7\text{Mn}_3\text{O}_x$  catalysts. These results indicate that the  $\text{Co}_5\text{Mn}_5\text{O}_x$  and  $\text{Co}_7\text{Mn}_3\text{O}_x$  catalysts have a much higher ability for forming nitrate species compared with the  $\text{MnO}_x$ ,  $\text{CoO}_x$  and  $\text{Co}_3\text{Mn}_7\text{O}_x$  catalysts, which is consistent with the  $\text{NO}_x$ -TPD results.

In order to study the reactivity of adsorbed nitrate/nitrite species, after the catalyst was exposed to the mixed gas of 500 ppm NO + 5 vol.%  $\text{O}_2/\text{Ar}$  (50 mL/min) at 100 °C for 90 min, Ar (50 mL/min) was first introduced to sweep the catalysts for 1 h and then replaced by 500 ppm  $\text{NH}_3/\text{Ar}$  at 100 °C. The in situ DRIFT spectra of the catalysts were collected at different times, as shown in Fig. 17. The results revealed that in the in situ DRIFT spectra of the  $\text{Co}_7\text{Mn}_3\text{O}_x$  catalyst, the intensity of the band at 1326  $\text{cm}^{-1}$  assigned to bidentate nitrate decreased with an increase in the exposure time of  $\text{NH}_3$ , indicating that bidentate nitrates are the reactive species for the SCR reaction. In contrast, the intensity of the band at 1450  $\text{cm}^{-1}$  assigned to ionic nitrate is hardly changed with an increase in the exposure time of  $\text{NH}_3$ , indicating that ionic nitrate are inactive in the SCR reaction. In the in situ DRIFT spectra of the  $\text{Co}_7\text{Mn}_3\text{O}_x$  catalyst, the intensity of the band at 1616  $\text{cm}^{-1}$  assigned to bridged nitrate, and the bands at 1500 and 1312  $\text{cm}^{-1}$  assigned to bidentate nitrate decreased with an increase in the exposure time of  $\text{NH}_3$ , indicating that both bridged and bidentate nitrates are the reactive species for the SCR reaction. Moreover, the decrease in the intensity of the bands is more distinct in the spectra of the  $\text{Co}_7\text{Mn}_3\text{O}_x$  catalyst compared with that of the  $\text{Co}_3\text{Mn}_7\text{O}_x$  catalyst, thus suggesting that the  $\text{Co}_7\text{Mn}_3\text{O}_x$  catalyst possesses a high activity. On the other hand, in the in situ DRIFT spectra of the  $\text{Co}_7\text{Mn}_3\text{O}_x$  catalyst, the bands at 1430 and 1176  $\text{cm}^{-1}$  assigned to  $\text{NH}_4^+$  ions formed on Brønsted acid sites [55–57], and coordinated  $\text{NH}_3$  adsorbed at Lewis acid sites [55,56,58] respectively, appeared and increased with the increase in the exposure time of  $\text{NH}_3$ . In contrary, at prolonged  $\text{NH}_3$  exposure times, seldom new peaks emerged in the spectrum of the  $\text{Co}_3\text{Mn}_7\text{O}_x$  catalyst, indicating that the  $\text{Co}_7\text{Mn}_3\text{O}_x$  catalyst has a higher ability for  $\text{NH}_3$  adsorption. These results are in good agreement with the  $\text{NH}_3$ -TPD results.

To explore the reaction scheme in depth, the reaction of  $\text{NH}_3$  species adsorbed on the  $\text{Co}_7\text{Mn}_3\text{O}_x$  catalyst surface in advance with the mixed gas of NO +  $\text{O}_2$  was also conducted and the results are shown in Fig. 18. The  $\text{Co}_7\text{Mn}_3\text{O}_x$  catalyst were first pretreated in Ar (50 mL/min) at 300 °C for 2 h and then cooled to 50 °C. Subsequently, the catalyst was exposed to 500 ppm  $\text{NH}_3/\text{Ar}$  (50 mL/min) at 50 °C, while in situ

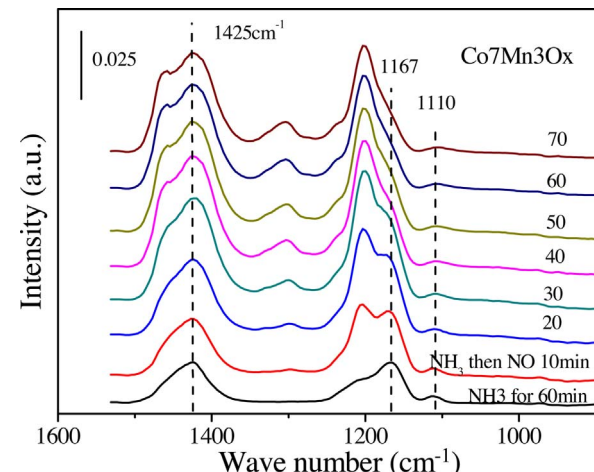
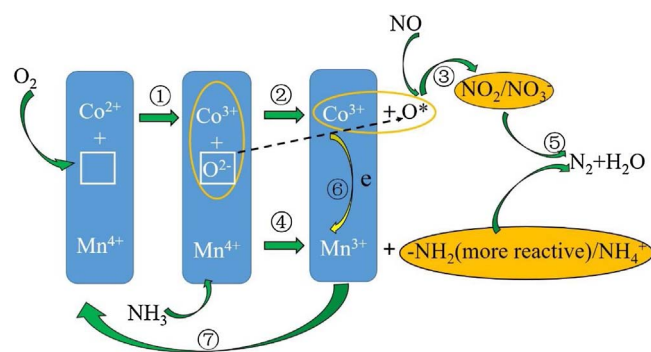


Fig. 18. In situ DRIFT spectra of the  $\text{Co}_7\text{Mn}_3\text{O}_x$  catalyst in the mixed gas of 500 ppm NO + 5 vol.%  $\text{O}_2/\text{Ar}$  for different times after adsorption of 500 ppm  $\text{NH}_3/\text{Ar}$  at 50 °C and blowing of Ar for 1 h.

DRIFT spectra of the catalysts were taken at different times. As shown in Fig. 18, after  $\text{NH}_3$  adsorption on the  $\text{Co}_7\text{Mn}_3\text{O}_x$  catalyst for 1 h, there are mainly three IR absorption bands at 1425, 1167 and 1110  $\text{cm}^{-1}$  in the spectrum of the  $\text{Co}_7\text{Mn}_3\text{O}_x$  catalyst. The former can be attributed to  $\text{NH}_4^+$  ions formed on Brønsted acid sites [55–57], and the latter two can be attributed to coordinated  $\text{NH}_3$  adsorbed at Lewis acid sites [55,56,58]. After the experiments of  $\text{NH}_3$  adsorption on the  $\text{Co}_7\text{Mn}_3\text{O}_x$  catalyst were performed, Ar (50 mL/min) was first introduced to sweep the catalysts at 50 °C for 1 h and was then replaced by 500 ppm NO + 5 vol.%  $\text{O}_2/\text{Ar}$  (50 mL/min), while in situ DRIFT spectra of the catalysts were collected at different times. As shown in Fig. 18, the bands at 1167 and 1110  $\text{cm}^{-1}$  disappeared gradually with the increase in the exposure time of NO +  $\text{O}_2$ , which indicate that coordinated  $\text{NH}_3$  adsorbed at Lewis acid sites have taken part in the SCR process. On the contrary, the bands at 1425  $\text{cm}^{-1}$  increased with the increase of the exposure time in NO +  $\text{O}_2$  due to the overlap in the signals of nitrite species and  $\text{NH}_4^+$  ions formed on Brønsted acid sites in this region. Therefore, the reactivity of  $\text{NH}_4^+$  ions formed on Brønsted acid sites is still a mystery.

#### 4. Discussion

It was reported that  $\text{MnO}_x$  has a high activity for  $\text{NH}_3$ -SCR at low temperature [14,34,35]. However, its thermal stability is poor [15,48]. Herein, a series of  $\text{Co}_a\text{Mn}_b\text{O}_x$  mixed oxides were prepared by the co-



**Scheme 1.** The proposed mechanism of the NH<sub>3</sub>-SCR reaction over the Co<sub>7</sub>Mn<sub>3</sub>O<sub>x</sub> catalyst and the synergistic catalytic effect between Mn and Co cations.

precipitation method to develop a highly efficient NH<sub>3</sub>-SCR catalyst along with a high thermal stability. The results show that the combination of Mn and Co to form a mixed oxide can dramatically enhance the NH<sub>3</sub>-SCR activity, and the activity of Co<sub>a</sub>Mn<sub>b</sub>O<sub>x</sub> mixed oxides is dependent on the Co/Mn molar ratio. The apparent energy barrier of Co<sub>3</sub>Mn<sub>7</sub>O<sub>x</sub> (19.3 kJ/mol), Co<sub>5</sub>Mn<sub>5</sub>O<sub>x</sub> (18.8 kJ/mol) and Co<sub>7</sub>Mn<sub>3</sub>O<sub>x</sub> (15.7 kJ/mol) are significantly lower than that of MnO<sub>x</sub> (33.9 kJ/mol) and CoO<sub>x</sub> (24.3 kJ/mol), and the Co<sub>7</sub>Mn<sub>3</sub>O<sub>x</sub> catalyst possessed the best NH<sub>3</sub>-SCR activity with an operation temperature window (80% NO<sub>x</sub> conversion) of 116–285 °C. Furthermore, the Co<sub>7</sub>Mn<sub>3</sub>O<sub>x</sub> catalyst exhibited a higher thermal stability, as well as excellent water- and sulfur-resistance performance compared with MnO<sub>x</sub>.

The crystal structure, phase state and specific surface area between the Co<sub>a</sub>Mn<sub>b</sub>O<sub>x</sub> and MnO<sub>x</sub> catalysts is significantly different, and those of the Co<sub>a</sub>Mn<sub>b</sub>O<sub>x</sub> catalysts are influenced by the composition. The Co<sub>7</sub>Mn<sub>3</sub>O<sub>x</sub> catalyst exhibited a large specific surface area due to its small particle size. As a result, the Co<sub>a</sub>Mn<sub>b</sub>O<sub>x</sub> catalysts possessed the high NH<sub>3</sub> and NO<sub>x</sub> adsorption ability, especially the Co<sub>7</sub>Mn<sub>3</sub>O<sub>x</sub> catalyst, which is beneficial to the high catalytic activity of the Co<sub>7</sub>Mn<sub>3</sub>O<sub>x</sub> catalyst in NH<sub>3</sub>-SCR. Furthermore, the NO<sub>x</sub> and NH<sub>3</sub> species formed on the Co<sub>a</sub>Mn<sub>b</sub>O<sub>x</sub> catalyst are different from that on MnO<sub>x</sub> and CoO<sub>x</sub> catalyst after the adsorption of NO<sub>x</sub> and NH<sub>3</sub>. Different NO<sub>x</sub> and NH<sub>3</sub> species generally played varied roles and have different performance in NH<sub>3</sub>-SCR reaction, leading to a significant improvement in SCR activity of the Co<sub>a</sub>Mn<sub>b</sub>O<sub>x</sub> catalyst [47,48]. On the other hand, the reducibility of the Co<sub>a</sub>Mn<sub>b</sub>O<sub>x</sub> catalysts is much better than those of the MnO<sub>x</sub> and CoO<sub>x</sub> catalysts. Moreover, the Co<sub>7</sub>Mn<sub>3</sub>O<sub>x</sub> catalyst has better oxygen mobility than MnO<sub>x</sub>, and consumed lattice oxygen can be quickly replenished by gaseous oxygen. In contrary, the Co<sub>3</sub>Mn<sub>7</sub>O<sub>x</sub>, Co<sub>5</sub>Mn<sub>5</sub>O<sub>x</sub> and Co<sub>7</sub>Mn<sub>3</sub>O<sub>x</sub> catalysts exhibited similar reducibility at low temperature (< 400 °C). Therefore, the Co<sub>a</sub>Mn<sub>b</sub>O<sub>x</sub> catalysts exhibited similar catalytic activities for NO oxidation at low temperature (< 200 °C), but are higher than those of the MnO<sub>x</sub> and CoO<sub>x</sub> catalysts. The high catalytic activity for NO oxidation can prompt the “fast SCR” reaction (NO + NO<sub>2</sub> + 2NH<sub>3</sub> → 2N<sub>2</sub> + 3H<sub>2</sub>O), leading to the increase in the NH<sub>3</sub>-SCR activity of the Co<sub>a</sub>Mn<sub>b</sub>O<sub>x</sub> catalysts.

As for the reaction mechanism, NO species could adsorb on the surface of the Co<sub>a</sub>Mn<sub>b</sub>O<sub>x</sub> and MnO<sub>x</sub> catalysts in the different form. Bidentate nitrate is dominant on the Co<sub>a</sub>Mn<sub>b</sub>O<sub>x</sub> catalyst, while bridged nitrate on the MnO<sub>x</sub> catalysts. Moreover, the Co<sub>5</sub>Mn<sub>5</sub>O<sub>x</sub> and Co<sub>7</sub>Mn<sub>3</sub>O<sub>x</sub> catalysts have a much higher ability for forming nitrate species compared with the MnO<sub>x</sub> and Co<sub>3</sub>Mn<sub>7</sub>O<sub>x</sub> catalysts. Both bidentate and bridged nitrates are the reactive species for the SCR reaction, whereas ionic nitrate are inactive in the SCR reaction. On the hand, coordinated NH<sub>3</sub> adsorbed at Lewis acid sites have been confirmed to take part in the SCR process. In contrary, the reactivity of NH<sub>4</sub><sup>+</sup> ions formed on Brønsted acid sites is still a mystery, due to the overlap in the signals of nitrite species and NH<sub>4</sub><sup>+</sup> ions formed on Brønsted acid sites in in situ DRIFT spectra.

Based on these abovementioned results, the reaction pathway of

NH<sub>3</sub>-SCR over the Co<sub>7</sub>Mn<sub>3</sub>O<sub>x</sub> catalyst can be proposed as shown in **Scheme 1**. Gaseous oxygen can be adsorbed and activated on oxygen vacancies (symbol □) and can be transformed into lattice oxygen O<sup>2-</sup> (Step 1), which can diffuse to the catalyst surface and act as surface active oxygen (O<sup>\*</sup>) during the SCR reaction (Step 2). Gaseous NO is adsorbed and then oxidized to NO<sub>2</sub>/NO<sub>3</sub><sup>-</sup> by O<sup>\*</sup> (Step 3), while NH<sub>3</sub> is activated by Mn<sup>4+</sup> to form NH<sub>2</sub> (higher activity confirmed by in situ DRIFT) and NH<sub>4</sub><sup>+</sup> (Step 4). Finally, NO<sub>2</sub>/NO<sub>3</sub><sup>-</sup> reacts with the NH species to produce N<sub>2</sub> and H<sub>2</sub>O (Step 5). The transformed Co<sup>3+</sup> and Mn<sup>3+</sup> are recovered by electron transfer (Step 6) and return to their original state (Step 7).

## 5. Conclusions

Co<sub>a</sub>Mn<sub>b</sub>O<sub>x</sub> catalysts prepared by the co-precipitation method were developed for NH<sub>3</sub>-SCR. The Co<sub>7</sub>Mn<sub>3</sub>O<sub>x</sub> catalyst with a Co/Mn molar ratio of 7/3 exhibited the optimal catalytic activity at low temperature, over which NO<sub>x</sub> conversion is greater than 80% at 116–285 °C. The apparent activation energy of the Co<sub>7</sub>Mn<sub>3</sub>O<sub>x</sub> catalyst was much smaller than that of MnO<sub>x</sub>, indicating that the active sites on the MnO<sub>x</sub> surface were altered due to the introduction of cobalt. In addition, the presence of cobalt can also enhance the thermal stability and the SO<sub>2</sub> and/or H<sub>2</sub>O resistance of MnO<sub>x</sub>. For instance, 5% H<sub>2</sub>O in the reactant gas has little influence on the activity of the Co<sub>7</sub>Mn<sub>3</sub>O<sub>x</sub> catalyst, and 62% NO can be removed after being poisoned by 50 ppm SO<sub>2</sub> for nearly 10 h. The deactivated catalysts can be totally regenerated by simply washing with water.

The Co<sub>a</sub>Mn<sub>b</sub>O<sub>x</sub> catalysts possess improved redox properties and more surface acid sites than either MnO<sub>x</sub> or CoO<sub>x</sub> alone due to synergistic effects between the Co and Mn species. In comparison with other Co<sub>a</sub>Mn<sub>b</sub>O<sub>x</sub> catalysts, the Co<sub>7</sub>Mn<sub>3</sub>O<sub>x</sub> catalyst has a higher adsorption ability for NH<sub>3</sub> and NO + O<sub>2</sub>, which is ascribed to the MnCo<sub>2</sub>O<sub>4.5</sub> phase and the higher surface area. Furthermore, the results of in situ DRIFT indicated that bridging nitrate and bidentate nitrate are the intermediate species in NH<sub>3</sub>-SCR. The high adsorption ability for NO + O<sub>2</sub> and improved redox properties of the Co<sub>7</sub>Mn<sub>3</sub>O<sub>x</sub> catalyst are beneficial for the formation of nitrate species on the catalyst surface to result in high SCR activity.

## Acknowledgments

This work was financially supported by the National Key Research and Development Program of China (2016YFC0204300), the National Key Basic Research Program of China (2013CB933200), the National Natural Science Foundation of China (21577034, 21333003), Science and Technology Commission of Shanghai Municipality (16ZR1407900) and Fundamental Research Funds for the Central Universities (WJ1514020, 222201717003).

## Appendix A. Supplementary data

Supplementary data associated with this article can be found, in the online version, at <http://dx.doi.org/10.1016/j.apcatb.2017.09.034>.

## References

- [1] D. Kwon, K. Nam, S. Hong, *Appl. Catal. B Environ.* 166–167 (2015) 37–44.
- [2] C. D'Agostino, S. Chansai, I. Bush, C. Gao, M.D. Mantle, C. Hardacre, S.L. James, L.F. Gladden, *Catal. Sci. Technol.* 6 (2015) 1661–1666.
- [3] V. Parvulescu, P. Grange, B. Delmon, *Catal. Today* 46 (1998) 233–316.
- [4] Z. Xiong, C. Wu, Q. Hu, H.Z. Wang, J. Jin, C.M. Liu, D.X. Guo, *Chem. Eng. J.* 286 (2016) 459–466.
- [5] N.Y. Topsøe, *Science* 265 (1994) 1217–1219.
- [6] T.J. Toops, J.A. Pihl, W.P. Partridge, *Fe-zeolite functionality, durability, and deactivation mechanisms in the selective catalytic reduction (SCR) of NO<sub>x</sub> with ammonia*, in: I. Nova, E. Tronconi (Eds.), *Urea-SCR Technology for DeNO<sub>x</sub> After Treatment of Diesel Exhausts*, Springer, New York, 2014, pp. 97–122.
- [7] J.H. Park, H.J. Park, J.H. Bak, I.S. Nam, C.H. Shin, J.H. Lee, B.K. Cho, S.H. Oh, J.

Catal. 240 (2006) 47–57.

[8] T.V.W. Janssens, H. Falsig, L.F. Lundsgaard, P.N.R. Vennestrøm, S.B. Rasmussen, P.G. Moses, F. Giordanino, E. Borfecchia, K.A. Lomachenko, C. Lamberti, S. Bordiga, A. Godiksen, S. Mossin, P. Beato, *ACS Catal.* 5 (2015) 2832–2845.

[9] L. Sun, Q. Cao, B. Hu, J. Li, J. Hao, G. Jing, X. Tang, *Appl. Catal. A Gen.* 393 (2011) 323–330.

[10] M. Kang, E.D. Park, J.M. Kim, J.E. Yie, *Catal. Today* 111 (2006) 236–241.

[11] C. Zhou, Y. Zhang, X. Wang, H. Xu, K. Sun, K. Shen, *J. Colloid Interface Sci.* 392 (2013) 319–324.

[12] S. Roy, B. Viswanath, M. Hegde, G. Madras, *J. Phys. Chem. C* 112 (2008) 6002–6012.

[13] D.A. Peña, B.S. Uphade, P.G. Smirniotis, *J. Catal.* 221 (2004) 421–431.

[14] M. Kang, E.D. Park, J.M. Kim, J.E. Yie, *Appl. Catal. A Gen.* 327 (2007) 261–269.

[15] D. Meng, W. Zhan, Y. Guo, Y. Guo, L. Wang, G. Lu, *J. Mol. Catal. A Chem.* 420 (2016) 272–281.

[16] W. Tian, H.S. Yang, X.Y. Fu, X.B. Zhang, *J. Hazard. Mater.* 188 (2011) 105–109.

[17] B. Meng, Z. Zhao, X. Wang, J. Liang, J. Qiu, *Appl. Catal. B Environ.* 129 (2013) 491–500.

[18] J.E. Park, E.D. Park, *Catal. Lett.* 144 (2014) 607–614.

[19] Y. Yan, L. Wang, H. Zhang, *Sep. Purif. Technol.* 175 (2017) 213–221.

[20] C. Zhang, C. Wang, W. Zhan, Y. Guo, Y. Guo, G. Lu, A. Baylet, A. Giroir-Fendler, *Appl. Catal. B Environ.* 129 (2013) 509–516.

[21] W. Tang, X. Wu, S. Li, W. Li, Y. Chen, *Cat. Commun.* 56 (2014) 134–138.

[22] W. Li, K. Xu, G. Song, X. Zhou, R. Zou, J. Yang, Z. Chen, J. Hu, *Cryst. Eng. Commun.* 16 (2014) 2335–2339.

[23] Y. Lu, W. Zhan, Y. He, Y. Wang, X. Kong, Q. Kuang, Z. Xie, L. Zheng, *ACS Appl. Mater. Interfaces* 6 (2014) 4186–4195.

[24] H. Zhou, L. Chen, V. Malik, C. Knies, D.M. Hofmann, K.P. Bhatti, S. Chaudhary, P.J. Klar, W. Heimbrodt, C. Klingshirn, *Phys. Status Solidi (A)* 204 (2007) 112–117.

[25] M. Richter, A. Trunschke, U. Bentrup, K.W. Brzezinka, E. Schreier, M. Schneider, M.M. Pohl, R. Fricke, *J. Catal.* 206 (2002) 98–113.

[26] R. Radhakrishnan, S.T. Oyama, *J. Catal.* 199 (2001) 282–290.

[27] Y.F. Han, K. Ramesh, L. Chen, E. Widjaja, S. Chilukoti, F. Che, *J. Phys. Chem. C* 111 (2007) 2830–2833.

[28] B. Fazio, L. Spadaro, G. Trunfio, J. Negro, F. Arena, *J. Raman Spectrosc.* 42 (2011) 1583–1588.

[29] Z. Chen, Q. Yang, H. Li, X. Li, L. Wang, S. Chi Tsang, *J. Catal.* 276 (2010) 56–65.

[30] H.-S. Kim, P.C. Stair, *J. Phys. Chem. B* 108 (2004) 17019–17026.

[31] Y.L. Zheng, W.Z. Wang, D. Jing, L. Zhang, *Chem. Eng. J.* 284 (2016) 21–27.

[32] X. Tang, J. Li, L. Sun, J. Hao, *Appl. Catal. B Environ.* 99 (2010) 156–162.

[33] L. Zhang, L. Shi, L. Huang, J. Zhang, R. Gao, D. Zhang, *ACS Catal.* 4 (2014) 1753–1763.

[34] S. Yang, C. Wang, J. Li, N. Yan, L. Ma, H. Chang, *Appl. Catal. B Environ.* 110 (2011) 71–80.

[35] J. Chen, M. Shen, X. Wang, G. Qi, J. Wang, W. Li, *Appl. Catal. B Environ.* 134–135 (2013) 251–257.

[36] D. Li, X. Liu, Q. Zhang, Y. Wang, H. Wan, *Catal. Lett.* 127 (2009) 377–385.

[37] Z. Lian, F. Liu, H. He, X. Shi, J. Mo, Z. Wu, *Chem. Eng. J.* 250 (2014) 390–398.

[38] Y.X. Su, B.X. Fan, L.S. Wang, Y.F. Liu, B.C. Huang, M.L. Fu, L.M. Chen, D.Q. Ye, *Catal. Today* 201 (2013) 115–121.

[39] Z.Q. Zou, M. Meng, Y.Q. Zha, *J. Phys. Chem. C* 114 (2010) 468–477.

[40] X.F. Tang, Y.G. Li, X.M. Huang, Y.D. Xu, H.Q. Zhu, J.G. Wang, W.J. Shen, *Appl. Catal. B Environ.* 62 (2006) 265–273.

[41] F. Kapteijn, L. Singoredjo, A. Andreini, J.A. Moulijn, *Appl. Catal. B Environ.* 25 (1994) 173–189.

[42] M.Z. Wu, W.C. Zhan, Y.L. Guo, Y. Guo, Y.S. Wang, L. Wang, G.Z. Lu, *Appl. Catal. A Gen.* 523 (2016) 97–106.

[43] A. Patel, P. Shukla, J.L. Chen, T.E. Rufford, V. Rudolph, Z.Z. Zhu, *Catal. Today* 212 (2013) 38–44.

[44] R.B. Jin, Y. Liu, Y. Wang, W.L. Cen, Z.B. Wu, H.Q. Wang, X.L. Weng, *Appl. Catal. B Environ.* 148–149 (2014) 582–588.

[45] M. Ruggeri, I. Nova, E. Tronconi, J.A. Pihl, T.J. Toops, W.P. Partridge, *Appl. Catal. B Environ.* 166–167 (2015) 181–192.

[46] H. Xu, Q. Zhang, C. Qiu, T. Lin, M. Gong, Y. Chen, *Chem. Eng. Sci.* 76 (2012) 120–128.

[47] F. Liu, H. He, Y. Ding, C. Zhang, *Appl. Catal. B Environ.* 93 (2009) 194–204.

[48] D. Meng, W. Zhan, Y. Guo, Y. Guo, L. Wang, G. Lu, *ACS Catal.* 5 (2015) 5973–5983.

[49] Q. Li, M. Meng, Z.-Q. Zou, X.-G. Li, Y.-Q. Zha, *J. Hazard. Mater.* 161 (2009) 366–372.

[50] S.M. Lee, S.C. Hong, *Appl. Catal. B* 163 (2015) 30–39.

[51] S. Liu, X.D. Wu, D. Weng, R. Ran, *Ind. Eng. Chem. Res.* 51 (2012) 2271–2279.

[52] I. Atribak, B. Azambre, A. Bueno López, A. García-García, *Appl. Catal. B Environ.* 92 (2009) 126–137.

[53] Z. Zhang, Y. Zhang, Q. Su, Z. Wang, Q. Li, X. Gao, *Environ. Sci. Technol.* 44 (2010) 8254–8258.

[54] G. Qi, R.T. Yang, *J. Phys. Chem. B* 108 (2004) 15738–15747.

[55] F. Liu, H. He, *J. Phys. Chem. C* 114 (2010) 16929–16936.

[56] D.A. Peña, B.S. Uphade, E.P. Reddy, P.G. Smirniotis, *J. Phys. Chem. B* 108 (2004) 9927–9936.

[57] N. Topsøe, H. Topsøe, J. Dumesic, *J. Catal.* 151 (1995) 226–240.

[58] H.K. Matralis, M. Ciardelli, M. Ruwet, P. Grange, *J. Catal.* 157 (1995) 368–379.